The impact of the South-East Madagascar bloom on the oceanic CO_2 sink.

Nicolas Metzl[1], Claire Lo Monaco[1], Coraline Leseurre[1], Céline Ridame[1], Jonathan Fin[1], Claude Mignon[1], Marion Gehlen[2], Thi Tuyet Trang Chau[2]

[1] Laboratoire LOCEAN/IPSL, Sorbonne Université-CNRS-IRD-MNHN, Paris, 75005, Fr

[2] Laboratoire LSCE/IPSL, CEA-CNRS-UVSQ, Université Paris-Saclay Gif-sur-Yvette, 91191, Fr

Correspondence to: Nicolas Metzl (nicolas.metzl@locean.ipsl.fr)

Abstract

We described new sea surface CO_2 observations in the southwestern Indian Ocean obtained in January 2020 when a strong bloom event occurred south-east of Madagascar and extended eastward in the oligotrophic Indian Ocean subtropical domain. Compared to previous years (1991-2019) we observed very low fCO_2 and dissolved inorganic carbon concentrations (C_T) in austral summer 2020, indicative of a biologically driven process. In the bloom the anomaly of fCO_2 and C_T reached respectively -33 µatm and -42 $µmol.kg^{-1}$ whereas no change is observed for alkalinity (A_T). In January 2020 we estimated a local maximum of air-sea CO_2 flux at 27°S of -6.9 $mmol.m^{-2}.d^{-1}$ (ocean sink) and -4.3 $mmol.m^{-2}.d^{-1}$ when averaging the flux in the band 26-30°S. In the domain 25-30°S/50-60°E we estimated that the bloom led to a regional carbon uptake of about -1 $TgC.month^{-1}$ in January 2020 whereas this region was previously recognized as an ocean CO_2 source or near equilibrium during this season. Using a neural network approach that reconstructs the monthly fCO_2 fields we estimated that when the bloom was at peak in December 2019 the CO_2 sink reached -3.1 (±1.0) $mmol.m^{-2}.d^{-1}$ in the band 25-30°S, i.e. the model captured the impact of the bloom. Integrated in the domain restricted to 25-30°S/50-60°E the region was a CO_2 sink in December 2019 of -0.8 $TgC.month^{-1}$ compared to a CO_2 source of +0.12 (± 0.10) $TgC.month^{-1}$ in December when averaged over the period 1996-2018. Consequently in 2019 this region was a stronger CO_2 annual sink of -8.8 $TgC.yr^{-1}$ compared to -7.0 (±0.5) $TgC.yr^{-1}$ averaged over 1996-2018. In austral summer 2019/2020, the bloom was likely controlled by relatively deep mixed-layer depth during preceding winter (July-September 2019) that would supply macro and/or micro-nutrients as iron to the surface layer to promote the bloom that started in November 2019 in two large rings in the Madagascar Basin. Based on measurements in January 2020, we observed relatively high N_2 fixation rates (up to 18 nmol $N.L^{-1}.d^{-1}$) suggesting that diazotrophs could play a role on the bloom in the nutrient depleted waters. The bloom event in austral summer 2020, along with the new carbonate system observations, represents a benchmark case for complex biogeochemical model sensitivity studies (including N_2-fixation process and iron supplies) for a better understanding on the origin and termination of this still "mysterious" sporadic bloom and its impact on ocean carbon uptake in the future.

1 Introduction

In the south-western subtropical Indian Ocean a phytoplankton bloom, called the South-East Madagascar Bloom (SEMB) occurs sporadically during austral summer (December-March, Fig. 1). Based on first years of SeaWIFS satellite Chlorophyll-a (Chl-a) observations in 1997-2001 the SEMB has been first recognized by Longhurst (2001) as the largest bloom in the subtropics, extending over 3000 x 1500 km in the Madagascar Basin. When the SEMB is well developed like in February-March 1999 (Longhurst, 2001), monthly mean Chl-a concentrations are higher than 0.5 $mg.m^{-3}$ within the bloom contrasting with the low Chl-a in the surrounding oligotrophic waters (< 0.05 $mg.m^{-3}$). For reasons still not fully understood, this bloom occurred in specific years (1997, 1999 and 2000) but was absent or moderate during a strong El Niño - Southern Oscillation (ENSO) event in 1998. Following the first study by Longhurst (2001), the frequency, extension, levels of Chl-a concentration and processes that would control the SEMB and its variability have been investigated in several studies (Srokosz et al, 2004; Uz, 2007; Wilson and Qiu 2008; Poulton et al 2009; Raj et al 2010; Huhn et al 2012; Srokosz and Quartly 2013). Most of these studies were based on Chl-a derived from remote sensing and altimetry. They all concluded the need for *in-situ* observations to understand the initiation, extend and termination of the SEMB. To our knowledge *in-situ* biogeochemical observations (Chl-a, phytoplanktonic species and nutrients) within the SEMB region were only obtained during the MadEx experiment in February 2005 (Poulton et al 2009; Srokosz and Quartly 2013) a year when the bloom was not well developed (e.g. Uz, 2007; Wilson and Qiu 2008). The MadEx cruise was conducted above the Madagascar ridge and west of 51°E in the Madagascar Basin. However, the eastward extension of the SEMB reached occasionally the central oligotrophic Indian subtropics (longitude 70°E, Fig. 1b) where the bloom is transported and apparently bounded by the South Indian Counter Current (SICC) around 25°S (Siedler et al 2006; Palastanga et al 2007; Huhn et al 2012; Menezes et al 2014). A recent analysis of the East Madagascar Current (EMC) and its retroflection near the southern tip of Madagascar also suggests that complex dynamic sometimes promotes the SEMB (Ramanantsoa et al 2021). Modelling studies also suggested an eastward propagation of the SEMB through advection or eddy transport originating from the south-east coast of Madagascar (Lévy et al 2007; Srokosz et al 2015; Dilmahamod, et al 2020) but a precise explanation of the internal (e.g. local upwelling, Ekman pumping, meso-scale dynamics) or external processes (e.g. iron from rivers, coastal zones or sediments) at the origin of this “mysterious” bloom is still missing.

The above studies have been recently synthetized by Dilmahamod et al (2019) who also proposed an index to determine the level of the SEMB (strong, moderate or absent) based on the difference in Chl-a concentrations between the western and eastern regions centered respectively around 55°E and 80°E at 24-28°S. Quoting Dilmahamod et al (2019): “The South-East Madagascar Bloom is one of the largest blooms in the world. It can play a major role in the fishing industry, as well as capturing carbon dioxide from the atmosphere”. Although numerous cruises measuring sea surface CO_2 fugacity (fCO_2) were conducted since the nineties in the south-western Indian Ocean region (Poisson et al., 1993; Metzl et al., 1995; Sabine et al 2000; Metzl, 2009), the impact of the SEMB on air-sea CO_2 fluxes was not previously investigated. This is probably because the bloom was not strong enough at the time of the cruises to identify large fCO_2 anomalies in this region. Therefore, the temporal (seasonal and/or inter-annual) fCO_2 variability in the western and subtropical Indian Ocean is generally interpreted by thermodynamics as the main control, biological activity and mixing processes being secondary driving processes in this oligotrophic region (Louanchi et al, 1996; Metzl et al 1998; Sabine et al 2000; Takahashi et al 2002). On the other hand, all climatologies based on observations suggest rather homogeneous sea surface fCO_2 or dissolved inorganic carbon (C_T) fields in this region (Takahashi et al, 2002, 2009, 2014; Lee et al, 2000; Sabine et al 2000; Bates et al 2006; Lauvset et al 2016; Zeng et al 2017; Broullón et al 2020; Keppler et al 2020; Fay et al 2021; Gregor and Gruber 2021). This suggests that, although the SEMB and its extent have been regularly observed since 1997 it seems to have a small effect on fCO_2 or C_T spatial variations. However, in austral summer 2019-2020, the SEMB was particularly pronounced reaching monthly mean Chl-a concentrations up to 2.5 $mg.m^{-3}$ at the peak of the bloom in December 2019. It was clearly much stronger than previously observed, at least since 1997 (Fig. 1) and reflected in fCO_2 observations in this region (Fig. 2).

In this analysis, we describe new oceanic carbonate system observations in surface waters obtained in January 2020 associated to this very strong SEMB event and compare these observations with climatological values and previous fCO_2 data when the SEMB was not well developed. We also evaluate the impact of the bloom on air-sea CO_2 fluxes based on both observations and reconstructed monthly fCO_2 fields in the South-Western Indian Ocean.

2 Data collection

As part of the long-term OISO project (Ocean Indien Service d'Observations), the OISO-30 cruise was conducted in austral summer 2020 (from 2-January to 6-February 2020) onboard the R.V. Marion-Dufresne in the Southern Indian Ocean (part of the track shown in Fig. 1). During the cruise, underway continuous surface measurements were obtained for temperature (SST), salinity (SSS), fugacity of CO_2 (fCO_2), total alkalinity (A_T) and total dissolved inorganic carbon (C_T). Analytical methods followed the protocol used since 1998 and previously described for other OISO cruises (e.g. Metzl et al 2006; Metzl, 2009; Lo Monaco et al, 2021). Sea surface temperature and salinity were measured continuously using a SBE45 thermosalinograph. Salinity data were controlled by regular sampling and conductivity measurements (Guildline Autosal 8400B and using IAPSO standard/OSIL). The SST and SSS data were also checked against CTD's surface records when available. Accuracies of SST and SSS are respectively 0.005 °C and 0.01. Total alkalinity (A_T) and total dissolved inorganic carbon (C_T) were measured continuously in surface water (3 to 4 sample/hour) using a potentiometric titration method (Edmond, 1970) in a closed cell. For calibration, we used the Certified Referenced Materials (CRMs, Batch #173) provided by Pr. A. Dickson (SIO, University of California). Replicate measurements were occasionally performed at the same location. At 30°S/54°E for 4 replicates the mean A_T and C_T concentrations were respectively 2328.6 (±0.7) and 1998.2 (±1.6) µmol.kg^{-1}. At 35°S/53.5°E for 6 replicates the mean A_T and C_T were 2340.5 (±0.6) and 2060.6 (±1.1) µmol.kg^{-1}. Overall, we estimated the accuracy for both A_T and C_T better than 3 µmol.kg^{-1} (based on the analysis of CRMs). Like for all other OISO cruises, the surface underway A_T and C_T data will be available at NCEI/OCADS (www.ncei.noaa.gov/access/ocean-carbon-data-system/oceans/VOS_Program/OISO.html).

For fCO_2 measurements, sea-surface water was continuously equilibrated with a "thin film" type equilibrator thermostated with surface seawater (Poisson *et al.*, 1993). The xCO_2 in the dried gas was measured with a non-dispersive infrared analyser (NDIR, Siemens Ultramat 6F). Standard gases for calibration (271.39, 350.75 and 489.94 ppm) were measured every 6 hours. To correct xCO_2 dry measurements to fCO_2 *in situ* data, we used polynomials given by Weiss and Price (1980) for vapour pressure and by Copin-Montégut (1988, 1989) for temperature (temperature in the equilibrium cell measured using SBE38 was on average 0.28°C warmer than SST during the OISO-30 cruise). The oceanic fCO_2 data for this cruise are available in the SOCAT data product (version v2021, Bakker et al., 2016, 2021) and at NCEI/OCADS (Lo Monaco and Metzl, 2021). Note that when added to SOCAT, the original fCO_2 data are recomputed (Pfeil et al., 2013) using temperature correction from Takahashi et al (1993). Given the small difference between SST and equilibrium temperature, the fCO_2 data from our cruises are identical (within 1 µatm) in SOCAT and NCEI/OCADS. For coherence with other cruises we used the fCO_2 values as provided by SOCAT.

During the OISO-30 cruise, silicate (Si) concentrations in surface and water column samples (filtered at 0.2 µm, poisoned with 100 µl $HgCl_2$ and stored at 5°C) were measured onshore by colorimetry (Aminot and Kérouel, 2007; Coverly et al. 2009). Based on replicate measurements for deep samples collected during OISO cruises we estimate an error of about 0.3 % in Si concentrations.

Unfiltered and 20µm-prefiltered seawater (~ 10m depth) were collected for the determination of net N_2 fixation in both the total fraction and the size-fraction lower than 20 µm using the $^{15}N_2$ gas-tracer addition method (Montoya et al., 1996). By difference, we calculated N_2 fixation rates related to the microphytoplankton size class (> 20µm). Immediately after sampling, 2.5ml of 99% $^{15}N_2$ (Eurisotop) were introduced to 2.3L polycarbonate bottles through a butyl septum. $^{15}N_2$ tracer was added to obtain a ~10% final enrichment. Then, each bottle was vigorously shaken and incubated in an on-deck incubator with circulating seawater and equipped with a blue filter to simulate the level of irradiance at the sampling depth. After 24h-incubation, 2.3L were filtered onto pre-combusted 25mm GF/F filters, and filters were stored at −25°C. Sample filters were dried at 40°C for 48h before analysis. Nitrogen (N) content of particulate matter and its ^{15}N isotopic ratio were quantified using an online continuous flow elemental analyzer (Flash 2000 HT), coupled with an Isotopic Ratio Mass Spectrometer (Delta V Advantage via a conflow IV interface from Thermo Fischer Scientific). N_2 fixation rates were calculated by isotope mass balanced as described by Montoya et al. (1996). The detection limit for N_2 fixation, calculated from significant enrichment and lowest particulate nitrogen is estimated to 0.04 nmol N L^{-1} d^{-1}.

Other data used in this analysis (e.g. Chl-a from remote sensing, ADCP, current fields, fCO_2, A_T, C_T from other cruises or from climatology) will be referred to in the next sections when appropriate.

3 Reconstructed fCO_2 and air-sea CO_2 fluxes

In order to complement the results based on regional *in-situ* data and evaluate the CO_2 sink anomalies in this region back to 1996, we also used results from a neural network model that reconstructs monthly fCO_2 fields and air-sea CO_2 fluxes. The fCO_2 fields were obtained from an ensemble-based feed-forward neural network model (named CMEMS-LSCE-FFNNN) described in Chau et al (2022). This ensemble-based approach is an updated and improved version of the model by Denvil-Sommer et al (2019). Model results are annually qualified and distributed by the European Copernicus Marine Environment Monitoring Service (CMEMS, Chau et al 2020). To take into account the period in austral summer 2020 when the SEMB was particularly strong, we used the latest temporal extension of the model which relies on the most recent version of the SOCAT data-base (SOCAT-v2021, Bakker et al, 2021). For a full description of the model, access to the data and a statistical evaluation of fCO_2 reconstructions please refer to Chau et al (2022).

4 Results

4.1 Sea surface fCO_2, C_T and A_T distributions in the SEMB in January 2020

In January 2020, the SEMB occupied a large region in the Southern section of the Mozambique Channel, the Natal Basin, the Mozambique Plateau and the Madagascar Basin. It extended eastward with meso-scale and filaments structures reaching 60°E in the southern subtropical Indian Ocean where Chl-a was up to 0.5 $mg.m^{-3}$ (Fig. 1a). Compared to previous years, the spatial structure of the 2020 SEMB event resembled to the one that occurred in 2008 (e.g. Dilmahamod et al 2019), albeit with much higher Chl-a concentrations in 2020 (Fig. 1b, c). As opposed to previous years, the 2020 SEMB event started in November 2019 in the Madagascar Basin and was pronounced in two large rings with monthly mean Chl-a concentrations reaching 1 $mg.m^{-3}$ at 25°S/52°E (Supp Mat Fig. S1). These large Chl-a rings were likely linked to eddies and/or to the retroflection of the South-East Madagascar current, SEMC (Lutjeharms 1988; Longhurst 2001; de Ruijter et al 2004; Ramanantsoa et al 2021) as seen in the surface currents fields in November 2019 (Supp Mat Fig. S2). In December 2019, the surface of the SEMB extended in all directions and a maximum monthly mean Chl-a concentration up to 2.9 $mg.m^{-3}$ was detected around 25°S/51.5°E (Supp Mat Fig. S1). The SEMB was less developed in late February 2020 (Supp Mat Fig. S1). Whatever the origin and multiple drivers of the SEMB in 2020 through internal or external forcing (Dilmahamod et al 2019) this rather strong biological event would significantly drawdown the C_T concentration and fCO_2 during several weeks from November 2019 to February 2020 in this region.

Along the OISO-30 cruise track at 54°E in January 2020, the underway surface measurements started at 26.5°S for fCO_2 and at 27°S for A_T and C_T. Along this track the sea surface Chl-a concentrations were relatively lower south of 27°S (0.2-0.4 $mg.m^{-3}$) than north of 27°S (0.8-1.2 $mg.m^{-3}$, Fig. 3a). This was associated with a rapid decrease in fCO_2 (Figure 3a) and salinity normalized C_T ($N\text{-}C_T = C_T*35/SSS$) concentration (Fig. 3b). Because there was a sharp gradient in salinity at that latitude (Supp Mat Fig. S3), no significant change was observed for salinity normalized A_T ($N\text{-}A_T = A_T*35/SSS$) along the track (Fig. 3b). The structure of the currents from November 2019 to January 2020 (Supp Mat Fig. S2 and Fig. S4) suggests that the extension of the bloom was linked to the retroflection of the SEMC occurring around 24-26°S, one of the forms of the SEMC retroflection defined by Ramanantsoa et al (2021) that would transport nutrients eastward in the Indian Ocean. The current field in January 2020 presents a complex meandering structure deflecting southward at 51°E and recirculating northward around 53°E (Supp Mat Fig. S4). Further east, at 54°E along the cruise track, the ADCP data recorded during the OISO-30 cruise revealed the presence of a relatively strong westward current (up to 40 $cm.s^{-1}$) centered around 28-29°S identified down to 600m. As opposed to the SEMC retroflection this westward current would bring high salinity and low nutrients from the subtropics.

The mean properties and differences within and out of the peak bloom are listed in Table 1. Although the ocean was warmer in the bloom at 27°S (about +1°C, Supp Mat Fig. S3), fCO_2 was clearly much lower at that location. The fCO_2 difference within and out of the peak bloom was -33 µatm based on fCO_2 measurements. Given the error associated to the fCO_2 calculations using A_T and C_T data (±13 µatm, Orr et al 2018) the observed fCO_2 difference is confirmed with fCO_2 calculated with the A_T-C_T pairs (difference of -34.5 µatm, last column in Table 1). If one takes into account the effect of the warming on fCO_2 (Takahashi et al, 1993), the fCO_2 in the bloom would be 323.5 µatm. Therefore the solely impact of the biological processes in the bloom reduced fCO_2 by -49.3 µatm. This is a very large effect and coherent with the observed difference in $N\text{-}C_T$ of -23.4 $\mu mol.kg^{-1}$ within and out of the bloom and almost no change in $N\text{-}A_T$ (Table 1).

The atmospheric xCO_2 was 410 ppm in January 2020, equivalent to 397 µatm for fCO_{2atm} (dashed line in Fig. 3a, where xCO_2 in ppm was corrected to fCO_2 according to Weiss and Price, 1980). Consequently the region was a strong CO_2 sink within the bloom area with maximal ΔfCO_2 value of -60 µatm at 27°S (where $\Delta fCO_2 = fCO_{2oce} - fCO_{2atm}$). As a comparison at this location (28-24°S-52.5°E) the climatological ΔfCO_2 value for January (Takahashi et al 2009) was estimated between +4 to +10 µatm, i.e. a small source or near equilibrium. It is well known that gas exchange at the air-sea interface depends on both ΔfCO_2 and the wind speed (e.g. Wanninkhof 2014). The net flux of CO_2 across the air-sea interface (FCO_2) was calculated according to the following equation (1):

$$FCO_2 = k\ K0\ \Delta fCO_2 \qquad \text{(Eq. 1)}$$

Where K0 is the solubility of CO_2 in seawater calculated from *in situ* temperature and salinity (Weiss, 1974) and k ($cm.h^{-1}$) is the gas transfer velocity expressed from the wind speed U ($m.s^{-1}$) (Wanninkhof, 2014) and the Schmidt number Sc (Wanninkhof, 1992) following equation (2):

$$k = 0.251\ U^2\ (Sc/660)^{-0.5} \qquad \text{(Eq. 2)}$$

In the region 25°S-30°S/45°E-60°E the average monthly wind speed (GMAO, 2015) was 7.9 $m.s^{-1}$ in January 2020. This value is the same as derived from 6-hourly wind speed products at location 27°S-54°E, 7.8 (±2.3) $m.s^{-1}$ (Supp Mat Fig. S5a). Using equation (1) and (2), this leads to a CO_2 sink of -6.9 $mmol.m^2.d^{-1}$ at 27°S in January 2020 whereas in the climatology (Takahashi et al 2009) this region was a CO_2 source of +0.72 $mmol.m^2.d^{-1}$ in January. In the band 26-30°S where Chl-a varied between 1.2 and 0.2 $mg.m^{-3}$ (Fig. 3) the CO_2 sink was still significant on average, -4.3 (± 1.3) $mmol.m^2.d^{-1}$.

Integrated over 1 month and a surface of the bloom of 3000x1500 km (Longhurst, 2001), i.e. 4.5 Mkm^2, the carbon uptake in January 2020 would be -7.2 (± 2.2) $TgC.month^{-1}$. However, based on the Chl-a distribution in January 2020 (Fig. 1a), we estimated the surface of the bloom east of 45°E to range between 1 and 1.7 Mkm^2 depending the criteria based on Chl-a concentrations (respectively Chl-a = 0.16 $mg.m^{-3}$ for a major bloom or Chl-a = 0.07 $mg.m^{-3}$ for a bloom, Dilmahamod et al 2019). This leads to an integrated CO_2 sink ranging between -1.7 and -2.7 $TgC.month^{-1}$ probably more realistic than when using the surface of the bloom as defined by Longhurst (2001). When restricted to the surface of the domain 25-30°S/50-60°E (0.6 Mkm^2) the integrated CO_2 sink in January 2020 based on fCO_2 observations would be -1.0 $TgC.month^{-1}$.

Given the fCO_2 distribution observed in January 2020 and the strong CO_2 sink evaluated within the SEMB, we then compared the 2020 observations with a period when the bloom was absent (or small) and for which fCO_2 data were also available for comparison.

4.2 Comparison with a low bloom year: 2005

For the period 1998-2016, Dilmahamod et al (2019) synthetized the season and years (their Table 1) with strong or moderate SEMB and years when no bloom was clearly observed, such as in 2005. This is confirmed from the Chl-a time series constructed around 27°S that showed low Chl-a in 2005 compared to 2004 and 2006 (Fig. 1 b, c). However, it is worth to note that Poulton et al (2009) and Srokosz and Quartly (2013) analyzed in-situ observations collected in this region in February 2005 during the MadEx cruise. They detected that the bloom was present albeit with low Chl-a concentrations (maximum of 0.2 $mg.m^{-3}$). Based on surface observations (Chl-a, species and nutrients) along a NE-SE transect between 47°E and 51°E, Srokosz and Quartly (2013) reported that Chl-a variability around 50°E was strongly linked to eddy field as first noticed by Longhurst (2001). They also observed from Seasoar fluorimeter data that the deep chlorophyll maximum (DCM) around 70-100m was relatively homogenous along the cruise track and not associated with eddy field as opposed to surface Chl-a. Excepted for silicate that showed some low "patchy" concentrations (<1 $\mu mol.kg^{-1}$) associated with filaments of higher Chl-a in the Madagascar Basin (Poulton et al, 2009), no significant variation was observed for other nutrients during MadEx in February 2005 and this was probably the case for fCO_2.

Here we revisited the SEMB in austral summer 2005 using data collected during the OISO-12 cruise (expocode 35MF20050113 in the SOCAT data product, Bakker et al, 2016). To compare with 2020, we selected the fCO_2 data collected along the same track around 54°E in February 2005 (note that the fCO_2 data collected in January 2005 to the east, around 60°E, were almost the same, not shown). In the region east of Madagascar, the bloom was discernible around 25°S in January 2005 with maximum Chl-a concentrations around 0.3 $mg.m^{-3}$ at 50°E (Supp. Mat. Fig. S6). In January, the bloom appeared to extend eastward following a large meandering structure around 25°S and in February 2005 the bloom is even detectable at 65°E-70°E where Chl-a concentration was on average 0.19 (± 0.03) $mg.m^{-3}$ within the core of the bloom. Interestingly this seems to be centered in the core of the SICC (Huhn et al 2012) as revealed at 25°S by the ADCP observations obtained in 2005 along the OISO-12 cruise track as well as in surface current fields (Supp. Mat. Fig. S7). Like in November 2019 (Supp. Mat. Fig. S2) there was a clear signal of the SEMC retroflection in January 2005 that could explain the structure and eastward propagation of the bloom. The retroflection located around 26°S-48°E in 2005 is close to the location of the so-called “early retroflection” defined by Ramanantsoa et al (2021) as opposed to the canonical retroflection of the SEMC found at the southern tip of Madagascar. The early retroflection of the SEMC would import nutrient-rich water from the coast in the Madagascar Basin and trigger the phytoplankton bloom.

The bloom in 2005 was low (Srokosz and Quartly, 2013; Dilmahamod et al, 2019) and thus it had no impact on the fCO_2 distribution. This is shown in Fig. 4 were we compared fCO_2 observations along the same track in February 2005 and January 2020. We present the results for ΔfCO_2 along with sea surface Chl-a for each period. In 2005 the sea surface fCO_2 was pretty homogeneous with values near the atmospheric fCO_2 level (ΔfCO_2 close to 0). Although one would expect to observe higher fCO_2 15 years later due to anthropogenic carbon uptake by the ocean driven by the increase in atmospheric CO_2 (and thus about the same ΔfCO_2), both fCO_2 and ΔfCO_2 in 2020 were much lower than in 2005 especially north of 27°S (Fig. 4, Table 2). In austral summer 2005, the region was near equilibrium with a ΔfCO_2 mean value of +8.6 (± 7.1) µatm. This is close to the climatology constructed for a reference year in 2005 (Takahashi et al, 2014, Table 2) and this is expected as the climatology included the fCO_2 data from OISO cruises obtained in this region in 1998-2008. On the opposite, in January 2020 we observed a strong sink (maximum ΔfCO_2 = -60 µatm at 27°S). As the temperature was about the same for both periods, the difference in fCO_2 was not due to thermodynamics and the CO_2 sink observed in 2020 was directly linked to the strong SEMB that occurred in austral summer.

The average monthly wind speed was also about the same in 2020 (7.9 $m.s^{-1}$) and 2005 (8.5 $m.s^{-1}$) (Supp Mat. Fig. S5b). Consequently the difference in the air-sea CO_2 flux between the two periods was controlled by ΔfCO_2. In the region 26-30°S/55°E, the mean CO_2 flux in 2005 was estimated at +1.2 $mmol.m^{-2}.d^{-1}$ (a source) against -4.3 $mmol.m^{-2}.d^{-1}$ (a sink) in 2020.

5 Discussion

5.1 A large biologically driven fCO_2 negative anomaly in 2020 relative to the anthropogenic uptake of CO_2

Like for fCO_2, the $N\text{-}C_T$ concentrations observed in the SEMB in January 2020 (1950 $\mu mol.kg^{-1}$, Fig. 3b, Table 1) were low compared to the climatology (Takahashi et al 2014). At 24°S-28°S/54°E, the $N\text{-}C_T$ climatological value in January range between 1970 and 1980 $\mu mol.kg^{-1}$. As the climatology produced by Takahashi et al (2014) was referred to a nominal year 2005, one would expect to observe higher $N\text{-}C_T$ concentrations in 2020 due to anthropogenic CO_2 uptake.

In the Indian Ocean the decadal change of anthropogenic CO2 (C_{ant}) was first evaluated by Peng et al (1998) comparing data obtained in 1978 and 1995 north of 20°S. For the upper layer in the tropics (20°S-10°S) Peng et al (1998) estimated an increasing rate of C_{ant} of around 1.1 $\mu mol.kg^{-1}.yr^{-1}$. More recently, Murata et al (2010) evaluated the changes of C_{ant} concentrations between 1995 and 2003 in the South Indian Ocean subtropics. They estimated a mean increase of C_{ant} of +7.9 (± 1.1) $\mu mol.kg^{-1}$ over 8.5 years in the upper layers that corresponds to a trend of +0.93 (± 0.13) $\mu mol.kg^{-1}.yr^{-1}$. In a global context, Gruber et al (2019 a, b) estimated an accumulation of anthropogenic CO_2 (C_{ant}) of +14.3 (± 0.3) $\mu mol.kg^{-1}$ in surface waters of the south-western Indian Ocean over 1994-2007, corresponding to an increasing rate in C_{ant} of +1.10 (± 0.02) µmol.kg^{-1}.yr^{-1}. To confirm these C_{ant} trends that were based on the C_{ant} differences between two periods (1995-1978, 2003-1995 or 2007-1994) we calculated the C_{ant} concentrations and long-term trend using water-column data available in 1978-2020 in the region 30-26°S/55°E. We extracted the data from the most recent GLODAP quality controlled data product (version GLODAPv2-2021, Lauvset et al 2021a,b) completed with data from OISO cruises in 2012-2018. To calculate C_{ant} we used the TrOCA method developed by Touratier et al. (2007). Because indirect methods are not suitable for evaluating C_{ant} concentrations in surface waters due to gas exchange and biological activity we selected the data in the layer 100-250m below the DCM. C_{ant} concentrations were calculated for each sample in that layer and then averaged for each period to estimate the trend (Fig. 5). As expected the C_{ant} concentrations in subsurface increased significantly from 1978 to 2020 and the long-term trend of +1.05 (± 0.08) µmol.kg^{-1}.yr^{-1} over this period is close to previous estimates based on different periods and approaches (Peng et al 1998; Murata et al, 2010; Gruber et al, 2019a).

Furthermore the C_{ant} trend of around +1 µmol.kg^{-1}.yr^{-1} is coherent with an increase in C_T of between +0.93 and +1.17 µmol.kg^{-1}.yr^{-1} derived from the oceanic fCO_2 increase over the period 1991-2007 estimated from winter and summer fCO_2 data (+1.75 and +2.2 µatm.yr^{-1} respectively, Metzl, 2009) assuming constant alkalinity and temperature. With the new data available after 2007, we have revisited the fCO_2 long-term trend by selecting only the austral summer data in the region around 27°S-55°E (Fig. 2). For the period 1991-2019 we estimated a fCO_2 trend of +1.55 (± 0.40) µatm.yr^{-1}. This is less than the atmospheric fCO_2 increase of +1.89 (± 0.03) µatm.yr^{-1} over the same period suggesting that the CO_2 sink increased at this location. In a broader context, Landschützer et al (2016) suggested that the carbon uptake tended to increase slightly in 1998-2011 in the Subtropical Indian Ocean (their figure 3). We will see that such a change in the CO_2 fluxes in this region is also revealed in the CMEMS-LSCE-FFNN model (Chau et al, 2022). Note that if at that location 27°S/55°E (Fig. 2) the ocean fCO_2 data in 2020 were also used to estimate the trend (1991-2020), the rate of fCO_2 would be only +1.09 (± 0.48) µatm.yr^{-1}. i.e. about half the atmospheric fCO_2 trend. The fCO_2 observations in 2020 represent a large negative anomaly at local scale and thus caution is needed when incorporating such an anomaly to detect and interpret long-term change in the CO_2 sink, at least in the south-western Subtropical Indian Ocean.

To compare the fCO_2 trends listed above with the anthropogenic rate of around +1.0 µmol.kg^{-1}.yr^{-1} (Fig. 5), we have calculated C_T from the fCO_2 data and A_T derived from salinity (described below). For this calculation we used the CO2sys program (version CO2sys_v2.5, Orr et al., 2018) developed by Lewis and Wallace (1998) and adapted by Pierrot et al. (2006) with K1 and K2 dissociation constants from Lueker et al. (2000) and KSO_4 constant from Dickson (1990). The total boron concentration is calculated according to Uppström (1974). For nutrients we fixed phosphate concentrations at 0 and silicate at 2.0 (± 0.6) µmol.kg^{-1} (the mean of 79 surface observations measured during previous OISO cruises in the region 22°S-30°S). To derive A_T from salinity we used the surface A_T observations obtained since 1998 in the subtropical south-western Indian Ocean (OISO cruises). From these data we estimated a robust relationship (Fig. 6):

$$A_T\,(\mu mol.kg^{-1}) = 62.1601 * SSS + 123.1 \quad (rms= 7.0\ \mu mol.kg^{-1},\ r= 0.89,\ n= 3400) \qquad \text{(Eq. 3)}$$

The use of other relationships (e.g. Millero et al 1998; Lee et al 2006) would change slightly the A_T concentrations but not the interpretation on the C_T trend in this region. The time-series of salinity normalized C_T ($N\text{-}C_T = C_T*35/SSS$) in the box 27°S-28°S/55°E shows that $N\text{-}C_T$ increased over the period 1991-2019 at a rate of +0.70 (± 0.24) µmol.kg^{-1}.yr^{-1} (Fig. 7). This is somehow lower than the anthropogenic trend of +1 µmol.kg^{-1}.yr^{-}

^{1} suggesting that in addition to the anthropogenic CO_2 uptake, natural processes could also have a small impact on the C_T and fCO_2 trends in surface waters over almost 30 years.

Having an estimate of the C_T change due to anthropogenic CO_2 (around +1 µmol.kg^{-1}.yr^{-1}) and taking into account this effect, the climatological N-C_T concentration of 1973 µmol.kg^{-1} for 2005 (Takahashi et al 2014) corrected for the year 2020 would be 1988 µmol.kg^{-1} in the region of interest. This is higher by up to +36 µmol.kg^{-1} than the observed N-C_T in January 2020 in the SEMB (Table 1, Fig. 7). When correcting the climatological value to the observed C_T trend of +0.7 µmol.kg^{-1}.yr^{-1}, the N-C_T in 2020 would be 1983.5 µmol.kg^{-1}, i.e. +32.5 µmol.kg^{-1} higher than the observed value in January 2020. The N-C_T anomaly in January 2020 is also large compared to the mean N-C_T seasonal amplitude of 20 µmol.kg^{-1} generally observed in the South Indian subtropics (Metzl et al 1998; Takahashi et al 2014). We also note that climatological N-A_T concentrations of 2295 µmol.kg^{-1} for January (Takahashi et al 2014) are very close to those we observed in January 2020 (Table 1, Fig. 3b). Therefore the low fCO_2 and strong CO_2 sink in 2020 in the SEMB is due to a large drawdown of C_T, i.e. not driven by temperature changes or alkalinity.

5.2 Specificities of the SEMB bloom in 2020

Based on previous studies it is likely that the biologically driven reduction of C_T in the SEMB under depleted sea surface nitrate concentrations was associated with the process of N_2 fixation (Uz, 2007). The hypothesis that diazotrophy would play a role in the temporal C_T (and thus fCO_2) variability is supported by the observation of large N_2-fixing phytoplankton in the SEMB region in 2005 during MadEx cruise (Poulton et al 2009). These authors found that the filamentous cyanobacteria *Trichodesmium* was most abundant south of Madagascar (over the Madagascar ridge) whereas diatom-diazotroph associations (as *Rhizosolenia/Richelia*) were mainly observed east of Madagascar (in the Madagascar Basin).

Our measurements in January 2020 showed high spatial variability of the N_2 fixation rate (range from 0.8 to 18.3 nmol N.L^{-1}.d^{-1}, Fig. 8). Such variability in the subtropical Indian ocean was also recently reported by Hörstmann et al (2021) who measured N_2 fixation rates between 0.7 and 7.9 nmol N.L^{-1}.d^{-1} in January-February 2017 in the same region (OISO-27 cruise) but when the SEMB was not pronounced (Fig. 1b, 1c) and when fCO_2 was high and above equilibrium (Fig. 2). Our results for silicate (Si) and N_2-fix observations are difficult to interpret because few samples were collected along the track (Fig. 8). A maximum of N_2 fixation rate was observed at 30°S that was not linked to changes in other properties. This local high N_2 fixation rate could be related to *Trichodesmium* species but it was not sampled in January 2020. We also noted low Si concentrations at 27°S (0.6 µmol.kg^{-1}) associated with higher Chl-a and lower fCO_2 and C_T (Fig. 3). The low silicate might be associated with the presence of diatom-diazotroph associations (DDA) as observed during the MadEx cruise (Poulton et al 2009). In the bloom N_2 fixation increased northward from 28°S (factor ~5). Based on measurements for different size fractions we observed that the N_2 fixation is mainly related to the fraction > 20µm (i.e. Trichodesmium and DDA) representing 88% (± 9%) of the N_2 fixation. “Hotspots” of large diazotrophs (20-180 and 180-2000 µm) were also detected in other regions of the south-western Indian Ocean in May 2010 during the TARA expedition (Pierella Karlusich et al, 2021).

At global scale, the presence of N_2-fixers in the south-western Indian Ocean has been detected from satellite data (Westberry and Siegel, 2006; Qi et al 2020) and relatively high N_2 fixation rates in austral summer in this region were also derived from N_2-fix data using a machine learning approach (Tang and Cassar, 2019; Tang et al, 2019). A large scale distribution of diazotrophy was further estimated from surface C_T observations suggesting the presence of N_2-fixers in the Mozambique Channel and the South-Western Indian Ocean (Lee et al, 2002; Ko et al, 2018). These authors used regional N-C_T versus SST relationships to reconstruct the N-C_T field from which they estimated the net carbon production (NCP) in nitrate depleted waters, a proxy for carbon production by N_2 fixing microorganisms. The N-C_T/SST relationship observed from in-situ data in January 2020 somehow mimics this process (Fig. 9), i.e. the inter-annual variability of the N-C_T/SST relationship would also inform on the NCP by N_2-fixers.

Sea surface warming and shallow mixed-layer depth (MLD) are proposed to lead to optimal conditions for the growth of the N_2-fixers and generate the SEMB (e.g. Longhurst, 2001; Srokosz et al 2015). In austral summer 2020, the ocean was not much warmer than previous years suggesting that temperature was not a specific driver of the SEMB that year. To the contrary, in January 2020 the region experienced a particularly shallow MLD which might have favored the bloom (observed MLD around 20m at 27°S-28°S, Supp. Mat. Fig. S8 and Fig. S9).

As noted above, the strong bloom started in November 2019 and could be well identified in two large rings (Supp. Mat. Fig. S1). In the northern ring at 25°S-52°E the MLD was deep (> 80m) during 3 consecutive months in July-September 2019 and deeper compared to previous years (Supp. Mat. Fig. S10). This would have injected nutrients (and maybe iron) in surface layers and when the MLD was shallow at that location (< 20 m) the bloom developed in November 2019 and reached high Chl-a in December 2019 (up to 1.8 mg.m^{-3}). As the bloom covered a large region in December 2019 and January 2020 other specific processes like iron supply (from dust, coastal zone, rivers or sediments) still need to be identified to fully explain 2020 SEMB dynamics. The 2020 bloom was clearly recognized in Chl-a, fCO_2 and C_T observations but at that stage we have no clear explanation on the process (or multiple drivers) that generated its extend and intensity.

5.3 The changing ocean CO_2 uptake in the SEMB based on reconstructed pCO2

The results presented above were based on local underway fCO_2 observations and the integrated air-sea CO_2 fluxes were thus extrapolated from local data on a surface representing the area covered by the bloom leading to a carbon uptake of between -1.7 and -2.7 TgC.$month^{-1}$ in January 2020. In the domain 25-30°S/50-60°E we estimated a CO_2 sink in January 2020 close to -1 TgC.$month^{-1}$.

To evaluate the impact of the bloom at the regional scale, we used monthly surface ocean pCO_2 and air-sea CO_2 flux fields reconstructed by a neural network method as described in section 3 (CMEMS-LSCE-FFNN, Chau et al, 2022). The SEMB was well developed in December 2019 and we can evaluate its impact on the air-sea CO_2 fluxes by comparing December 2018 (low bloom) and December 2019 (strong bloom, Fig. 10). In the region 25-30°S/50-60°E, the average pCO_2 in December 2019 (375.9 ±6.3 µatm) was much lower than in December 2018 (396.6 ±6.0 µatm) and thus opposite of the expected pCO_2 increase due to anthropogenic CO_2 uptake. At the local scale, within the bloom at 27°S-54°E or at 29°S-50°E the CMEMS-LSCE-FFNN model estimated low pCO_2 clearly linked to higher Chl-a in December 2019 (Supp. Mat. Fig. S11 and Fig. S12). Consequently the region was a small CO_2 source of +0.07 (± 0.53) mmol.m^{-2}.d^{-1} in December 2018 but a CO_2 sink in December 2019 of -3.1 (± 1.0) mmol.m^{-2}.d^{-1}. Integrated over the region 25-30°S/50-60°E the carbon uptake changed from a small CO_2 source in December 2018 of +0.019 TgC.$month^{-1}$ to a CO_2 sink in December 2019 of -0.8 TgC.$month^{-1}$ (Supp Mat Fig. S13) close to the estimate derived from observations in January 2020 (-1.0 TgC.$month^{-1}$). Over the period 1996-2018, the model evaluates each year a CO_2 source in December averaging +0.12 (± 0.10) TgC.$month^{-1}$. This suggests that in late 2019 the CMEMS-LSCE-FFNN model did capture the effect of the SEMB on pCO_2 and CO_2 fluxes, leading to a stronger regional CO_2 annual sink in 2019 (-8.8 TgC.yr^{-1}) compared to previous years (Fig. 11). A major SEMB was previously recognized in 1999, 2006 and 2008 (Dilmahamod et al 2019; see also Fig. 1). The model overestimates the CO_2 sink in 2006 and 2008 but surprisingly not in 1999 (Fig. 11). This is probably because the ocean was warmer from December 1998 to Mach 1999 inducing a positive anomaly of fCO_2 that would balance the decrease of fCO_2 due to the biological activity in summer 1999. With the exception of 2008 when the SEMB was also strong (Fig. 1) the CO_2 sink anomalies in 1998-2018 appeared relatively modest compared to that observed in 2019 (Fig. 11).

6. Conclusions

The new observations in the South-Western Indian Ocean presented here showed that the fCO_2 and C_T concentrations in January 2020 were very low and far from normal conditions since 1991. This is explained by the strong SEMB event that started in November 2019 in this region and was well developed in December 2019 and January 2020. Thanks to the continuous ocean color satellite data since 1997, the time-series of Chl-a in this region showed that the bloom was particularly strong in austral summer 2019/2020. We suspect that prior to 1997, the SEMB has been less intense as suggested by *in-situ* fCO_2 data in 1991-1994 (Fig. 2). We estimated that the SEMB led to a regional carbon uptake of between -1.7 and –2.7 $TgC.month^{-1}$ in January 2020. The variation of the regional ocean CO_2 sink due to the SEMB developed in late 2019 was also quantified with the CMEMS-LSCE-FFNN model. Model results indicate a large anomaly in December 2019 that led to an annual sink of -8.8 $TgC.yr^{-1}$, i.e. about 1 $TgC.yr^{-1}$ larger than previous years. The strong bloom in austral summer 2020 represents an interesting benchmark case to test models for a better understanding of the origin of the SEMB and its impact on the regional ocean CO_2 sink. Future studies should target sensitivity analysis with complex biogeochemical models including the CO_2 system, at different spatial resolution for the dynamics, and with (or without) N_2 fixers (e.g. Monteiro et al 2010; Landolfi et al 2015; Paulsen et al 2017). This plankton functional type is not yet included to models dedicated to this region (Srokosz et al 2015, Dilmahamod et al 2020). The new fCO_2, C_T, A_T and N_2 fixation rate observations presented here along with historical data (e.g. SOCAT, Bakker et al 2016, 2021, Fig. 2) could serve as a validation to compare periods with or without bloom. In the future, if the SEMB as observed in 2020 is more frequent or becomes a regular situation and if organic matter is exported below the surface mixed layer, this could represent a negative feedback to the ocean carbon cycle, i.e. the ocean sink would be enhanced. As already noted by several authors (e.g. Dilmahamod et al 2019) dedicated studies in this region at the scale of eddies coupling dynamical and biological processes, including the sampling of plankton, nutrients (e. g. iron), but also the determination of rates (e.g. N_2-fixation) etc… would be relevant to understand the processes controlling the SEMB and to evaluate its impact on the biological carbon pump.

Data availability

Data used in this study are available in SOCAT (www.socat.info) for fCO_2 surface data, in GLODAP (www.glodap.info) for water-column data, at NCEI/OCADS (www.ncei.noaa.gov/access/ocean-carbon-data-system/oceans/VOS_Program/OISO.html) for A_T-C_T surface data, at Jas-ADCP (http://uhslc.soest.hawaii.edu/sadcp) for ADCP data. The CMEMS-LSCE-FFNN model data are available at E.U. Copernicus Marine Service Information (https://resources.marine.copernicus.eu/products).

Authors contributions

CLM and NM are co-Is of the ongoing OISO project. fCO_2, A_T and C_T data for OISO-30 were measured by CLM, CL and CM and qualified by CLM and NM. Nutrients data for OIS0-30 were measured and qualified by

CL. N_2-fix data for OIS0-30 were measured and qualified by CR. CLM, NM, and JF qualified fCO_2, A_T and C_T data for previous OISO cruises. MG and TTTC developed the CMEMS-LSCE-FFNN model and provided the model results. NM started the analysis, wrote the draft of the manuscript and prepared the figures with contributions from all authors.

Competing interest

The authors declare that they have no conflict of interest.

Acknowledgments

The OISO program was supported by the French institutes INSU (Institut National des Sciences de l'Univers) and IPEV (Institut Polaire Paul-Emile Victor), OSU Ecce-Terra (at Sorbonne Université), and the French program SOERE/Great-Gases. We thank the French oceanographic fleet ("Flotte océanographique française") for financial and logistic support to the OISO program and the OISO-30 oceanographic campaign (https://doi.org/10.17600/18000679). We thank the captains and crew of *R.R.V. Marion Dufresne* and the staff at IFREMER, GENAVIR and IPEV. N_2 fixation analysis was also supported by the French Research Program LEFE (Les Enveloppes Fluides et l'Environnement) through ITALIANO project and we thank Magloire Mandeng-Yogo and Fethiye Cetin for the measurements performed at the ALYSES plate-form (OSU Ecce-Terra). The development of the neural network model benefited from funding by the French INSU-GMMC project "PPR-Green-Grog (grant no 5-DS-PPR-GGREOG), the EU H2020 project AtlantOS (grant no 633211), as well as through the Copernicus Marine Environment Monitoring Service (project 83-CMEMS-TAC-MOB). The Surface Ocean CO_2 Atlas (SOCAT, www.socat.info) is an international effort, endorsed by the International Ocean Carbon Coordination Project (IOCCP), the Surface Ocean Lower Atmosphere Study (SOLAS) and the Integrated Marine Biogeochemistry and Ecosystem Research program (IMBER), to deliver a uniformly quality-controlled surface ocean CO2 database. We thank Meric Srokosz and Ahmad Fehmi Dilmahamod for their fast reviews and suggestions and the associate editor Peter Landschützer to manage this manuscript.

References

Aminot, A. and R. Kérouel: Dosage automatique des nutriments dans les eaux marines. Méthodes en flux continu. Ed Ifremer-Quae, 188 p., ISBN-13 978-2-7592-0023-8, 2007

Bakker, D. C. E., Pfeil, B., Landa, C. S., Metzl, N., O'Brien, K. M., Olsen, A., Smith, K., Cosca, C., Harasawa, S., Jones, S. D., Nakaoka, S.-I., Nojiri, Y., Schuster, U., Steinhoff, T., Sweeney, C., Takahashi, T., Tilbrook, B., Wada, C., Wanninkhof, R., Alin, S. R., Balestrini, C. F., Barbero, L., Bates, N. R., Bianchi, A. A., Bonou, F., Boutin, J., Bozec, Y., Burger, E. F., Cai, W.-J., Castle, R. D., Chen, L., Chierici, M., Currie, K., Evans, W., Featherstone, C., Feely, R. A., Fransson, A., Goyet, C., Greenwood, N., Gregor, L., Hankin, S., Hardman-Mountford, N. J., Harlay, J., Hauck, J., Hoppema, M., Humphreys, M. P., Hunt, C. W., Huss, B., Ibánhez, J. S. P., Johannessen, T., Keeling, R., Kitidis, V., Körtzinger, A., Kozyr, A., Krasakopoulou, E., Kuwata, A., Landschützer, P., Lauvset, S. K., Lefèvre, N., Lo Monaco, C., Manke, A., Mathis, J. T., Merlivat, L., Millero, F. J., Monteiro, P. M. S., Munro, D. R., Murata, A., Newberger, T., Omar, A. M., Ono, T., Paterson, K., Pearce, D., Pierrot, D., Robbins, L. L., Saito, S., Salisbury, J., Schlitzer, R., Schneider, B., Schweitzer, R., Sieger, R., Skjelvan, I., Sullivan, K. F., Sutherland, S. C., Sutton, A. J., Tadokoro, K., Telszewski, M., Tuma, M., Van Heuven, S. M. A. C., Vandemark, D., Ward, B., Watson, A. J., and Xu, S. : A multi-decade record of high-quality fCO_2 data in version 3 of the Surface Ocean CO_2 Atlas (SOCAT), Earth Syst. Sci. Data, 8, 383-413, doi:10.5194/essd-8-383-2016, 2016.

Bakker, D. C. E. et al.. Surface Ocean CO2 Atlas Database Version 2021 (SOCATv2021) (NCEI Accession 0210711). NOAA National Centers for Environmental Information. Dataset. https://doi.org/10.25921/4xkx-ss49. 2021. Last Access 15/6/2021.

Bates, N. R., A. C. Pequignet, and C. L. Sabine: Ocean carbon cycling in the Indian Ocean: 1. Spatiotemporal variability of inorganic carbon and air-sea CO2 gas exchange, Global Biogeochem. Cycles, 20, GB3020, doi:10.1029/2005GB002491, 2006.

Broullón, D., Pérez, F. F., Velo, A., Hoppema, M., Olsen, A., Takahashi, T., Key, R. M., Tanhua, T., Santana-Casiano, J. M., and Kozyr, A.: A global monthly climatology of oceanic total dissolved inorganic carbon: a neural network approach, Earth Syst. Sci. Data, 12, 1725–1743, https://doi.org/10.5194/essd-12-1725-2020, 2020.

Chau, T. T. T., Gehlen, M., and Chevallier, F.: QUALITY INFORMATION DOCUMENT for Global Ocean Surface Carbon Product MULTIOBS_GLO_BIO_CARBON_SURFACE_REP_015_008, Res. Rap. Lab. Sci. Clim. Environ., 25, https://catalogue.marine.copernicus.eu/documents/QUID/CMEMS-MOB-QUID-015-008.pdf, 2020.

Chau, T. T. T., Gehlen, M., and Chevallier, F.: A seamless ensemble-based reconstruction of surface ocean pCO_2 and air–sea CO_2 fluxes over the global coastal and open oceans, Biogeosciences, https://doi.org/10.5194/bg-2021-207, in press, 2022.

Copin-Montégut, C.: A new formula for the effect of temperature on the partial pressure of CO_2 in seawater. *Marine Chemistry*, 25, 29-37. https://doi.org/10.1016/0304-4203(88)90012-6, 1988.

Copin-Montégut, C.: A new formula for the effect of temperature on the partial pressure of CO_2 in seawater. Corrigendum. *Marine Chemistry*, 27, 143-144. https://doi.org/10.1016/0304-4203(89)90034-0, 1989.

Coverly, S. C., Aminot, A., and R. Kérouel: Nutrients in Seawater Using Segmented Flow Analysis, In: Practical Guidelines for the Analysis of Seawater, Edited by: Oliver Wurl, CRC Press, https://doi.org/10.1201/9781420073072, 2009.

Denvil-Sommer, A., Gehlen, M., Vrac, M., and Mejia, C.: LSCE-FFNN-v1: a two-step neural network model for the reconstruction of surface ocean pCO_2 over the global ocean, Geosci. Model Dev., 12, 2091-2105, https://doi.org/10.5194/gmd-12-2091-2019, 2019.

de Ruijter, W. P. M., H. M. van Aken, E. J. Beier et al.: Eddies and dipoles around South Madagascar: Formation, pathways and large-scale impacts, Deep Sea Res., Part I, 51, 383–400, https://doi.org/10.1016/j.dsr.2003.10.011, 2004.

Dickson, A. G.: Standard potential of the reaction: AgCl(s) + ½H2(g) = Ag(s) + HCl(aq), and the standard acidity constant of the ion HSO4– in synthetic sea water from 273.15 to 318.15 K. *J. Chem. Thermodyn.* **22**: 113–127. doi:10.1016/0021-9614(90)90074-Z, 1990.

Dilmahamod, A. F., Penven, P., Aguiar-González, B., Reason, C. J. C., & Hermes, J. C.: A new definition of the South-East Madagascar Bloom and analysis of its variability. *Journal of Geophysical Research: Oceans*, *124*, 1717–1735. https://doi.org/10.1029/2018JC014582, 2019

Dilmahamod, A. F., Penven, P., Aguiar-Gonzalez, B., Reason, C. J. C., & Hermes, J. C.: A model investigation of the influences of the South-East Madagascar current on the South-East Madagascar bloom. *Journal of Geophysical Research: Oceans*, *125*, e2019JC015761. https://doi.org/10.1029/2019JC015761, 2020.

Edmond, J. M.: High precision determination of titration alkalinity and total carbon dioxide content of sea water by potentiometric titration, *Deep-Sea Res*., 17, 737–750, https://doi.org/10.1016/0011-7471(70)90038-0, 1970.

Fay, A. R., Gregor, L., Landschützer, P., McKinley, G. A., Gruber, N., Gehlen, M., Iida, Y., Laruelle, G. G., Rödenbeck, C., and Zeng, J.: Harmonization of global surface ocean pCO_2 mapped products and their flux calculations; an improved estimate of the ocean carbon sink, Earth Syst. Sci. Data Discuss. [preprint], https://doi.org/10.5194/essd-2021-16, in review, 2021.

GMAO, Global Modeling and Assimilation Office: MERRA-2 tavgM_2d_flx_Nx: 2d, Monthly mean, Time-Averaged, Single-Level, Assimilation, Surface Flux Diagnostics V5.12.4, Greenbelt, MD, USA, Goddard Earth Sciences Data and Information Services Center (GES DISC), Accessed: [*19/4/2021*], 10.5067/0JRLVL8YV2Y4, 2015.

Gregor, L. and Gruber, N.: OceanSODA-ETHZ: a global gridded data set of the surface ocean carbonate system for seasonal to decadal studies of ocean acidification, Earth Syst. Sci. Data, 13, 777–808, https://doi.org/10.5194/essd-13-777-2021, 2021.

Gruber, N., D. Clement, B. R. Carter, R. A. Feely, S. van Heuven, M. Hoppema, M. Ishii, R. M. Key, A. Kozyr, S. K. Lauvset, C. Lo Monaco, J. T. Mathis, A. Murata, A. Olsen, F. F. Perez, C. L. Sabine, T. Tanhua, and R. Wanninkhof: The oceanic sink for anthropogenic CO_2 from 1994 to 2007, *Science* vol. 363 (issue 6432), pp. 1193-1199. DOI: 10.1126/science.aau5153, 2019a

Gruber, N., Clement, D., Carter, B. R., Feely, R. A., Heuven, S. van, Hoppema, M., Ishii, M., Key, R. M., Kozyr, A., Lauvset, S. K., Lo Monaco, C., Mathis, J. T., Murata, A., Olsen, A., Perez, F. F., Sabine, C. L., Tanhua, T. and Wanninkhof, R.: The oceanic sink for anthropogenic CO2 from 1994 to 2007 - the data (NCEI Accession 0186034). NOAA National Centers for Environmental Information. Dataset. https://doi.org/10.25921/wdn2-pt10, 2019b [last acces 17/02/2020].

Hörstmann, C., Raes, E. J., Buttigieg, P. L., Lo Monaco, C., John, U., and Waite, A. M.: Hydrographic fronts shape productivity, nitrogen fixation, and microbial community composition in the southern Indian Ocean and the Southern Ocean, Biogeosciences, 18, 3733–3749, https://doi.org/10.5194/bg-18-3733-2021, 2021.

Huhn, F., A. von Kameke, V. Pérez-Muñuzuri, M. J. Olascoaga, and F. J. Beron-Vera: The impact of advective transport by the South Indian Ocean countercurrent on the Madagascar bloom, Geophys. Res. Lett., 39, doi:10.1029/2012GL051246, 2012.

Keppler, L., Landschützer, P., Gruber, N., Lauvset, S. K., & Stemmler, I.: Seasonal carbon dynamics in the near-global ocean. *Global Biogeochemical Cycles*, 34, e2020GB006571. doi:10.1029/2020GB006571, 2020.

Ko, Y. H., Lee, K., Takahashi, T., Karl, D. M., Kang, S.-H., & Lee, E.: Carbon-based estimate of nitrogen fixation-derived net community production in N-depleted ocean gyres. *Global Biogeochemical Cycles*, 32. Doi:10.1029/2017GB005634, 2018.

Landolfi, A., Koeve, W., Dietze, H., Kähler, P., & Oschlies, A.: A new perspective on environmental controls of marine nitrogen fixation. Geophysical Research Letters, 42, 4482–4489. https://doi.org/10.1002/2015GL063756, 2015.

Landschützer P., N. Gruber, and D. Bakker: Decadal variations and trends of the global ocean carbon sink, Global Biogeochem. Cycles, 30, *doi:*10.1002/2015GB005359, 2016.

Lauvset, S. K, R. M. Key, A. Olsen, S. van Heuven, A. Velo, X. Lin, C. Schirnick, A. Kozyr, T. Tanhua, M. Hoppema, S. Jutterström, R. Steinfeldt, E. Jeansson, M. Ishii, F. F. Pérez, T. Suzuki & S. Watelet: A new global interior ocean mapped climatology: the 1°x1° GLODAP version 2. Earth Syst. Sci. Data, 8, 325-340, doi:10.5194/essd-8-325-2016, 2016.

Lauvset, S. K., Lange, N., Tanhua, T., Bittig, H. C., Olsen, A., Kozyr, A., Álvarez, M., Becker, S., Brown, P. J., Carter, B. R., Cotrim da Cunha, L., Feely, R. A., van Heuven, S., Hoppema, M., Ishii, M., Jeansson, E., Jutterström, S., Jones, S. D., Karlsen, M. K., Lo Monaco, C., Michaelis, P., Murata, A., Pérez, F. F., Pfeil, B., Schirnick, C., Steinfeldt, R., Suzuki, T., Tilbrook, B., Velo, A., Wanninkhof, R., Woosley, R. J., and Key, R. M.: An updated version of the global interior ocean biogeochemical data product, GLODAPv2.2021, Earth Syst. Sci. Data Discuss. [preprint], https://doi.org/10.5194/essd-2021-234, in review, 2021a.

Lauvset, Siv K.; Lange, Nico; Tanhua, Toste; Bittig, Henry C.; Olsen, Are; Kozyr, Alex; Álvarez, Marta; Becker, Susan; Brown, Peter J.; Carter, Brendan R.; Cotrim da Cunha, Leticia; Feely, Richard A.; van Heuven, Steven M. A. C.; Hoppema, Mario; Ishii, Masao; Jeansson, Emil; Jutterström, Sara; Jones, Steve D.; Karlsen, Maren K.; Lo Monaco, Claire; Michaelis, Patrick; Murata, Akihiko; Pérez, Fiz F.; Pfeil, Benjamin; Schirnick, Carsten; Steinfeldt, Reiner; Suzuki, Toru; Tilbrook, Bronte; Velo, Antón; Wanninkhof, Rik; Woosley, Ryan J.; Key, Robert M.: Global Ocean Data Analysis Project version 2.2021 (GLODAPv2.2021) (NCEI Accession 0237935). [subset used GLODAPv2.2021_Indian_Ocean.cvs]. NOAA National Centers for Environmental Information. Dataset. https://doi.org/10.25921/ttgq-n825., 2021b. Accessed 2/8/2021.

Lee, K., Wanninkhof, R., Feely, R. A., Millero, F. J., & Peng, T. H.: Global relationships of total inorganic carbon with temperature and nitrate in surface seawater. Global Biogeochemical Cycles, 14(3), 979–994. https://doi.org/10.1029/1998GB001087, 2000.

Lee, K., Karl, D. M., Wanninkhof, R., & Zhang, J. Z.: Global estimates of net carbon production in the nitrate-depleted tropical and subtropical oceans. Geophysical Research Letters, 29(19), 1907. https://doi.org/10.1029/2001GL014198, 2002.

Lee, K., Tong, L.T., Millero, F.J., Sabine, C.L., Dickson, A.G., Goyet, C., Park, G.H., Wanninkhof, R., Feely, R.A., and Key, R.M.: Global relationships of total alkalinity with salinity and temperature in surface waters of the world's oceans. *Geophys. Res. Lett.* 33, L19605. doi10.1029/2006GL027207, 2006.

Lévy, M., Shankar, D., André, J.M., Shenoi, S. S., Durand, F., & de Boyer Montegut, C.: Basin-wide seasonal evolution of the Indian Ocean's phytoplankton blooms. *Journal of Geophysical Research*, *112*, C12014. https://doi.org/10.1029/2007JC004090, 2007.

Lewis E. and D. W. R. Wallace: Program developed for CO2 system calculations. ORNL/CDIAC-105. Carbon Dioxide Information Analysis Center, Oak Ridge National Laboratory, US. Dept. of Energy, Oak Ridge, TN, 1998.

Lo Monaco, C. and N. Metzl: Surface underway measurements of partial pressure of carbon dioxide (pCO2), salinity, temperature and other associated parameters during the R/V Marion Dufresne OISO-30 cruise (EXPOCODE 35MV20200106) in Indian Ocean from 2020-01-06 to 2020-02-01 (NCEI Accession 0223954). [indicate subset used]. NOAA National Centers for Environmental Information. Dataset. https://www.ncei.noaa.gov/archive/accession/0223954, 2021. Accessed 15-01-2021.

Lo Monaco, C., Metzl, N., Fin, J., Mignon, C., Cuet, P., Douville, E., Gehlen, M., Trang Chau, T.T., and Tribollet, A.: Distribution and long-term change of the sea surface carbonate system in the Mozambique Channel (1963-2019), *Deep-Sea Research Part II*, https://doi.org/10.1016/j.dsr2.2021.104936, 2021.

Longhurst, A.: A major seasonal phytoplankton bloom in the Madagascar Basin. *Deep-Sea Research Part I: Oceanographic Research Papers*, *48*(11), 2413–2422. https://doi.org/10.1016/S0967-0637(01)00024-3, 2001.

Louanchi, F., N. Metzl, and A. Poisson : Modelling the monthly sea surface fCO2 fields in the Indian Ocean. *Marine Chemistry*, 55, 265-279. https://doi.org/10.1016/S0304-4203(96)00066-7, 1996.

Lueker, T.J., Dickson, A.G., Keeling, C.D.: Ocean pCO(2) calculated from dissolved inorganic carbon, alkalinity, and equations for K-1 and K-2: validation based on laboratory measurements of CO2 in gas and seawater at equilibrium. *Marine Chemistry* 70, 105-119. https://doi.org/10.1016/S0304-4203(00)00022-0, 2000.

Lutjeharms, J.R.E.: Remote sensing corroboration of retroflection of the East Madagascar Current. Deep Sea Res. 35, 2045–2050. https://doi.org/10.1016/0198-0149(88)90124-0, 1988.

Menezes, V. V., H. E. Phillips, A. Schiller, N. L. Bindoff, C. M. Domingues, and M. L. Vianna: South Indian countercurrent and associated fronts, J. Geophys. Res. Oceans, 119, 6763–6791, doi:10.1002/2014JC010076, 2014.

Metzl, N., A. Poisson, F. Louanchi, C. Brunet, B. Schauer & B. Bres: Spatio-temporal distributions of air-sea fluxes of CO_2 in the Indian and Antarctic oceans, *Tellus B: Chemical and Physical Meteorology*, 47:1-2, 56-69, doi:10.3402/tellusb.v47i1-2.16006, 1995.

Metzl, N., F. Louanchi, and A. Poisson: Seasonal and interannual variations of sea surface carbon dioxide in the subtropical indian ocean. *Marine Chemistry*, 60, 131-146. https://doi.org/10.1016/S0304-4203(98)00083-8, 1998.

Metzl, N., C. Brunet, A. Jabaud-Jan, A. Poisson and B. Schauer: Summer and winter air-sea CO2 fluxes in the Southern Ocean *Deep Sea Res I*, 53, 1548-1563, doi:10.1016/j.dsr.2006.07.006, 2006.

Metzl, N.: Decadal increase of oceanic carbon dioxide in the Southern Indian Ocean surface waters (1991-2007). *Deep Sea Research Part II: Topical Studies in Oceanography*, 56, 8–10, 607-619. https://doi.org/10.1016/j.dsr2.2008.12.007, 2009.

Millero, F. J., Lee, K. and Roche, M.: Distribution of alkalinity in the surface waters of the major oceans. *Mar. Chem.* **60**, 111–130. https://doi.org/10.1016/S0304-4203(97)00084-4, 1998.

Monteiro, F. M., M. J. Follows, and S. Dutkiewicz: Distribution of diverse nitrogen fixers in the global ocean, Global Biogeochem. Cycles, 24, GB3017, doi:10.1029/2009GB003731, 2010.

Montoya, J. P., Voss, M., Kahler, P., and Capone, D. G.: A simple, high-precision, high-sensitivity tracer assay for N2 fixation, Appl. Environ. Microb., 62, 986–993, https://doi.org/10.1128/aem.62.3.986-993.1996, 1996

Murata, A., Kumamoto, Y., Sasaki, K., Watanabe, S., & Fukasawa, M.: Decadal increases in anthropogenic CO2 along 20°S in the South Indian Ocean. *Journal of Geophysical Research*, *115*, C12055. https://doi.org/10.1029/2010JC006250, 2010.

Orr, J. C., J.-M. Epitalon, A. G. Dickson and J.–P. Gattuso: Routine uncertainty propagation for the marine carbon dioxide system, *Marine Chemistry*, Vol. 207, 84-107, doi:10.1016/j.marchem.2018.10.006, 2018.

Palastanga, V., P. J. van Leeuwen, M. W. Schouten, and W. P. M. de Ruijter: Flow structure and variability in the subtropical Indian Ocean: Instability of the South Indian Ocean Countercurrent, J. Geophys. Res., 112, C01001, doi:10.1029/2005JC003395, 2007.

Paulsen, H., Ilyina, T., Six, K. D., & Stemmler, I.: Incorporating a prognostic representation of marine nitrogen fixers into the global ocean biogeochemical model HAMOCC. Journal of Advances in Modeling Earth Systems, 9, 438–464. https://doi.org/10.1002/2016MS000737, 2017.

Peng, T H., Wanninkhof, R., Bullister, J. *et al.*: Quantification of decadal anthropogenic CO_2 uptake in the ocean based on dissolved inorganic carbon measurements. *Nature,* 396, 560–563. doi:10.1038/25103, 1998.

Pfeil, B., Olsen, A., Bakker, D. C. E., Hankin, S., Koyuk, H., Kozyr, A., Malczyk, J., Manke, A., Metzl, N., Sabine, C. L., Akl, J., Alin, S. R., Bates, N., Bellerby, R. G. J., Borges, A., Boutin,J., Brown, P. J., Cai, W.-J., Chavez, F. P., Chen, A., Cosca, C., Fassbender, A. J., Feely, R. A., González-Dávila, M., Goyet, C., Hales, B., Hardman-Mountford, N., Heinze, C., Hood, M., Hoppema, M., Hunt, C. W., Hydes, D., Ishii, M., Johannessen, T., Jones, S. D., Key, R. M., Körtzinger, A., Landschützer, P., Lauvset, S. K., Lefèvre, N., Lenton, A., Lourantou, A., Merlivat, L., Midorikawa, T., Mintrop, L., Miyazaki, C., Murata, A., Nakadate, A., Nakano, Y., Nakaoka, S., Nojiri, Y., Omar, A. M., Padin, X. A., Park, G.-H., Paterson, K., Perez, F. F., Pierrot, D., Poisson, A., Ríos, A. F., Santana-Casiano, J. M., Salisbury, J., Sarma, V. V. S. S., Schlitzer, R., Schneider, B., Schuster, U., Sieger, R., Skjelvan, I., Steinhoff, T., Suzuki, T., Takahashi, T., Tedesco, K., Telszewski, M., Thomas, H., Tilbrook, B., Tjiputra, J., Vandemark, D., Veness, T., Wanninkhof, R., Watson, A. J., Weiss, R., Wong, C. S., and Yoshikawa-Inoue, H.: A uniform, quality controlled Surface Ocean CO2 Atlas (SOCAT), Earth Syst. Sci. Data, 5, 125-143, doi:10.5194/essd-5-125-2013, 2013.

Pierella Karlusich, J.J., Pelletier, E., Lombard, F. *et al.*: Global distribution patterns of marine nitrogen-fixers by imaging and molecular methods. *Nat. Commun.,* 12**,** 4160. doi:10.1038/s41467-021-24299-y, 2021.

Pierrot, D., E. Lewis, and D. W. R. Wallace: MS Excel Program Developed for CO2 System Calculations ORNL/CDIAC-105, Carbon Dioxide Inf. Anal. Cent., Oak Ridge Natl. Lab., U. S. Dept. of Energy, Oak Ridge, Tenn., 2006.

Poisson, A., Metzl, N., Brunet, C., Schauer, B., Bres, B., Ruiz-Pino, D., and Louanchi, F.: Variability of sources and sinks of CO_2 in the western Indian and southern oceans during the year 1991, *J. Geophys. Res.*, 98(C12), 22759– 22778, doi:10.1029/93JC02501, 1993.

Poulton, A. J., M. C. Stinchcombe, and G. D. Quartly: High numbers of Trichodesmium and diazotrophic diatoms in the southwest Indian Ocean, Geophys. Res. Lett., 36, L15610, doi:10.1029/2009GL0397179, 2009.

Qi, L., C. Hu, K. Mikelsons, M. Wang, V. Lance, S. Sun, B. B. Barnes, J. Zhao, and D. Van der Zande: In search of floating algae and other organisms in global oceans and lakes. Remote Sensing of Environment, 239,111659, https://doi.org/10.1016/j.rse.2020.111659, 2020.

Raj, R. P., Peter, B. N., & Pushpadas, D.: Oceanic and atmospheric influences on the variability of phytoplankton bloom in the Southwestern Indian Ocean. *Journal of Marine Systems*, *82*(4), 217–229. https://doi.org/10.1016/j.jmarsys.2010.05.009, 2010.

Ramanantsoa, J. D., Penven, P., Raj, R. P., Renault, L., Ponsoni, L., Ostrowski, M., et al.. Where and how the East Madagascar Current retroflection originates. *Journal of Geophysical Research: Oceans*, 126, e2020JC016203. https://doi.org/10.1029/2020JC016203, 2021

Sabine, C. L., R. Wanninkhof, R. M. Key, C. Goyet, and F. J. Millero: Seasonal CO2 fluxes in the tropical and subtropical Indian Ocean, *Mar. Chem.*, 72, 33–53. https://doi.org/10.1016/S0304-4203(00)00064-5, 2000.

Schlitzer, R, 2013. Ocean Data View, http:/odv.awi.de.

Siedler, G., M. Rouault, and J. R. E. Lutjeharms: Structure and origin of the subtropical South Indian Ocean Countercurrent, Geophys. Res. Lett., 33, L24609, doi:10.1029/2006GL027399, 2006.

Srokosz, M. A., Quartly, G. D., & Buck, J. J. H.: A possible plankton wave in the Indian Ocean. *Geophysical Research Letters*, *31*, L13301. https://doi.org/10.1029/2004GL019738, 2004.

Srokosz, M. A., & Quartly, G. D.: The Madagascar Bloom: A serendipitous study. *Journal of Geophysical Research: Oceans*, *118*, 14–25. https://doi.org/10.1029/2012JC008339, 2013.

Srokosz, M. A., Robinson, J.,McGrain, H., Popova, E. E., & Yool, A.: Could the Madagascar bloom be fertilized by Madagascan iron? *Journal of Geophysical Research: Oceans*, *120*, 5790–5803. https://doi.org/10.1002/2015JC011075, 2015.

Takahashi, T., Olafsson, J., Goddard, J. G., Chipman, D. W., and Sutherland, S. C.: Seasonal variation of CO2 and nutrients in the high-latitude surface oceans: A comparative study, *Global Biogeochem. Cycles*, 7(4), 843–878, doi:10.1029/93GB02263, 1993.

Takahashi, T., Sutherland, S. C., Sweeney, C., Poisson, A., Metzl, N., Tilbrook, B., Bates, N., Wanninkhof, R., Feely, R. A., Sabine, C., Olafsson, J., and Nojiri, Y.: Global Sea-Air CO2 Flux Based on Climatological Surface Ocean pCO2, and Seasonal Biological and Temperature Effect. *Deep-Sea Res. II*, 49, 9-10, 1601-1622, https://doi.org/10.1016/S0967-0645(02)00003-6, 2002.

Takahashi, T., Sutherland, S. C., Wanninkhof, R., Sweeney, C., Feely, R. A., Chipman, D. W., Hales, B., Friederich, G., Chavez, F., Sabine, C., Watson, A. J., Bakker, D. C., Schuster, U., Metzl, N., Yoshikawa-Inoue, H., Ishii, M., Midorikawa, T., Nojiri, Y., Körtzinger, A., Steinhoff, T., Hoppema, M., Olafsson, J., Arnarson, T. S., Tilbrook, B., Johannessen, T., Olsen, A., Bellerby, R., Wong, C., Delille, B., Bates, N., and de Baar, H. J.: Climatological mean and decadal change in surface ocean pCO2, and net sea air CO2 flux over the global oceans. *Deep-Sea Res. II*,56(8-10), 554–577, http://dx.doi.org/10.1016/j.dsr2.2008.12.009, 2009.

Takahashi, T., Sutherland, S. C., Chipman, D. W., Goddard, J. G., Ho, C., Newberger, T., Sweeney, C. and Munro, D. R.: Climatological distributions of pH, pCO2, total CO2, alkalinity, and CaCO3 saturation in the global surface ocean, and temporal changes at selected locations. *Marine Chemistry*, 164, 95–125, doi:10.1016/j.marchem.2014.06.004, 2014.

Tang, W., & Cassar, N.: Data-driven modeling of the distribution of diazotrophs in the global ocean. *Geophysical Research Letters*, *46*, 12,258–12,269. https://doi.org/10.1029/2019GL084376, 2019.

Tang, W., Li, Z., & Cassar, N.: Machine learning estimates of global marine nitrogen fixation. Journal of Geophysical Research: Biogeosciences, 124, 717–730. https://doi.org/10.1029/2018JG004828. 2019.

Touratier, F., Azouzi, L. and Goyet, C.: CFC-11, Δ14C and 3H tracers as a means to assess anthropogenic CO2 concentrations in the ocean. *Tellus B*, 59(2), 318–325, doi:10.1111/j.1600-0889.2006.00247.x, 2007.

Uppström, L. R.: The boron/chlorinity ratio of deep-sea water from the Pacific Ocean, Deep Sea Research and Oceanographic Abstracts, 21, 161–162, https://doi.org/10.1016/0011-7471(74)90074-6, 1974.

Uz, B. M.: What causes the sporadic phytoplankton bloom southeast of Madagascar? *Journal of Geophysical Research*, *112*, C09010. https://doi.org/10.1029/2006JC003685, 2007

Wanninkhof, R.: Relationship between wind speed and gas exchange over the ocean, J. *Geophys. Res., 97(C5)*, 7373–7382, doi:10.1029/92JC00188, 1992.

Wanninkhof, R.: Relationship between wind speed and gas exchange over the ocean revisited, Limnol. Oceanogr. Methods, 12, 351–362, doi:10.4319/lom.2014.12.351, 2014.

Weiss, R. F.: Carbon dioxide in water and seawater: The solubility of a non-ideal gas, Mar. Chem., 2, 203–215, doi:10.1016/0304-4203(74)90015-2, 1974.

Weiss, R. F. and Price, B. A.: Nitrous oxide solubility in water and seawater. *Marine Chemistry*, 8(4), 347–359, doi:10.1016/0304-4203(80)90024-9, 1980.

Westberry, T. K., and D. A. Siegel: Spatial and temporal distribution of Trichodesmium blooms in the world's oceans, *Global Biogeochem. Cycles*, 20, GB4016, doi:10.1029/2005GB002673, 2006.

Wilson, C., and X. Qiu: Global distribution of summer chlorophyll blooms in the oligotrophic gyres, Prog. Oceanogr., 78, 107–134. https://doi.org/10.1016/j.pocean.2008.05.002, 2008

Zeng, J., Matsunaga, T., Saigusa, N., Shirai, T., Nakaoka, S.-I., and Tan, Z.-H.: Technical note: Evaluation of three machine learning models for surface ocean CO_2 mapping, *Ocean Sci.*, 13, 303-313, doi:10.5194/os-13-303-2017, 2017.

Tables

Table 1: Mean properties and their difference observed in January 2020 within and out of the SEMB peak bloom. For fCO_2, results based on measurements (fCO_{2mes}) or calculated using A_T-C_T pairs (fCO_{2cal}) are both listed. Standard deviations are indicated between brackets.

Region	SST °C	SSS PSU	Chl-a $mg.m^{-3}$	C_T $\mu mol.kg^{-1}$	N-C_T $\mu mol.kg^{-1}$	A_T $\mu mol.kg^{-1}$	N-A_T $\mu mol.kg^{-1}$	fCO_{2mes} µatm	fCO_{2cal} µatm
Within Peak Bloom	26.39	35.22	0.97	1958.6	1951.7	2313.5	2305.4	339.5	329.8
(Around 27°S)	(0.21)	(0.05)	(0.18)	(2.5)	(1.0)	(2.7)	(0.7)	(2.5)	(2.0)
South of the Peak Bloom	25.32	35.48	0.41	2000.6	1975.2	2332.1	2302.4	372.8	364.3
(Around 28°S)	(0.10)	(0.03)	(0.04)	(2.2)	(1.4)	(1.9)	(1.3)	(2.2)	(2.6)
Difference In-Out	+1.07	-0.26	+0.56	-42.0	-23.4	-18.6	+3.0	-33.3	-34.5

Table 2: Mean sea surface properties observed along the same track in January 2020 and February 2005 in the region 30°S-26°S/54°E. Also indicated the mean values in the same region and season from the climatology of Takahashi et al (2014) and the Chl-a climatology evaluated for January-February 1998-2019. Nb is the number of observations for SST, SSS and fCO_2. Standard deviations are indicated in bracket.

Cruise	Period	SST (°C)	SSS (PSU)	fCO_2 (µatm)	ΔfCO_2 (µatm)	Chl-a ($mg.m^{-3}$)
OISO-12	Feb-2005	25.443	35.240	374.2	+8.6	0.087
Nb= 115		(0.813)	(0.112)	(7.1)	(7.1)	(0.014)
OISO-30	Jan-2020	25.103	35.442	362.2	-36.2	0.489
Nb=217		(0.739)	(0.110)	(10.7)	(10.7)	(0.266)
Climatology	Jan-Feb	26.242	35.230	376.1	+10.5	0.105
		(0.898)	(0.140)	(3.6)	(3.6)	(0.093)

Figures:

Figure 1: (a): Map of monthly surface Chl-a (mg.m^{-3}) in the South-Western Indian Ocean in January 2020 derived from MODIS data (4x4km resolution), highlighting the bloom South and South-East of Madagascar. (b) Hovmoller Time-series (Time/Longitude) of Chl-a (mg.m^{-3}) around 26.5°S along 50-70°E (Orange box in a). c) Time-series of monthly Chl-a (mg.m^{-3}) in the box 27°S/54.5°E (only when valid number of pixels is greater than 5 for each point). The orange line on the map identifies the track of the OISO-30 cruise. The figures highlight the high Chl-a concentration in austral summer 2020. Figures (a) and (b) produced with ODV (Schlitzer, 2013) from data downloaded at https://resources.marine.copernicus.eu/ (OCEANCOLOUR_GLO_CHL_L4_REP_OBSERVATIONS_009_093), last access, 10-April-2021.

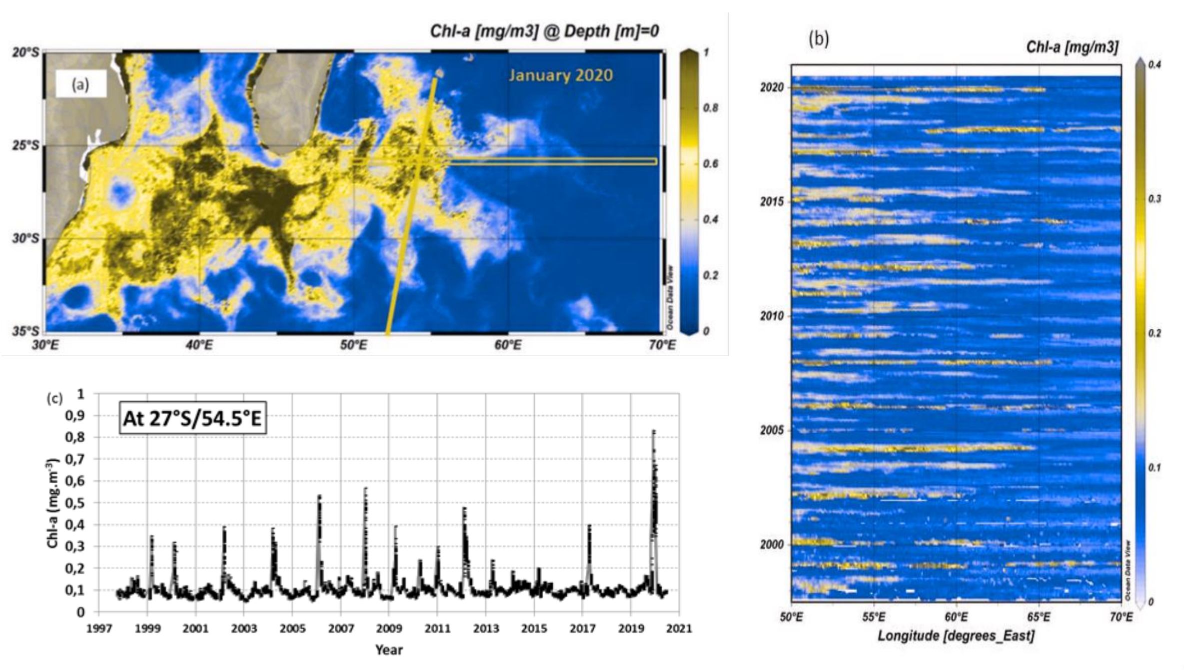

Figure 2: Left: Tracks of cruises with sea surface fCO_2 data available in the South-Western Indian Ocean in SOCAT data product (version SOCAT-v2021, Bakker et al, 2016; 2021). Right: Time-series of fCO_2 data (black dots) and mean fCO_2 for each period (grey triangles) in the box 27°S-28°S/55°E (black square in the map and insert on the right) for the months of January and February (data available from 1991 to 2020 for austral summer). The red curve is the atmospheric fCO_2. Although over 1991-2019 the ocean fCO_2 increased by +1.55 (± 0.40) µatm.yr^{-1} (dashed grey line) due to anthropogenic CO_2 uptake, the fCO_2 recorded in January 2020 in the bloom were low compared to previous years with some values below 340 µatm, i.e. lower than in 1991. The January-February averaged fCO_2 in the same region derived from the 2005 climatology of Takahashi et al (2014) is also plotted (orange diamond). Map on the left produced with ODV (Schlitzer, 2013).

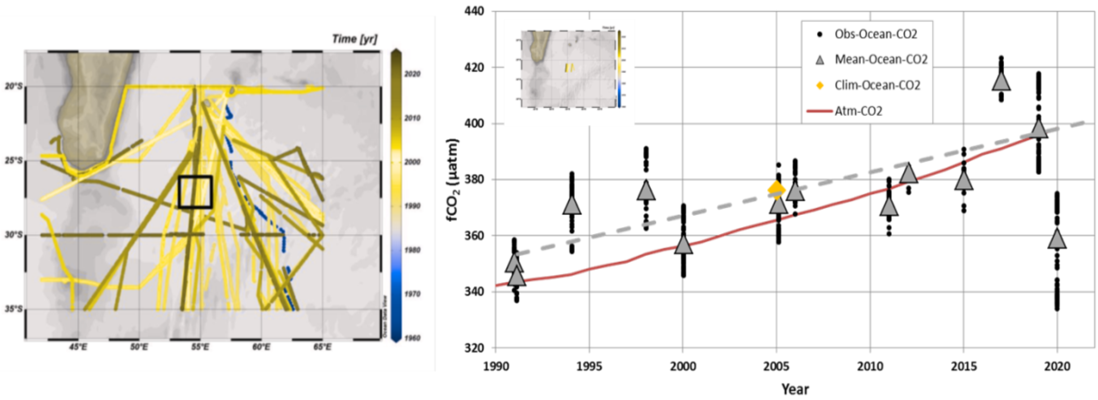

Figure 3: Top (a): Sea surface fCO_2 (µatm) measured in January 2020 (black circles) and Chl-a ($mg.m^{-3}$) from MODIS (4x4 km) along the cruise track (grey triangles). Bottom (b): Sea surface salinity normalized C_T (N-C_T, open circles) and salinity normalized A_T (N-A_T, black squares) measured in January 2020 (both in $\mu mol.kg^{-1}$). Low fCO_2 and N-C_T concentrations recorded around 27°S were linked to high Chl-a (up to 1.2 $mg.m^{-3}$) in the SEMB. In (a) the dashed-line represents the average atmospheric fCO_2 for January 2020.

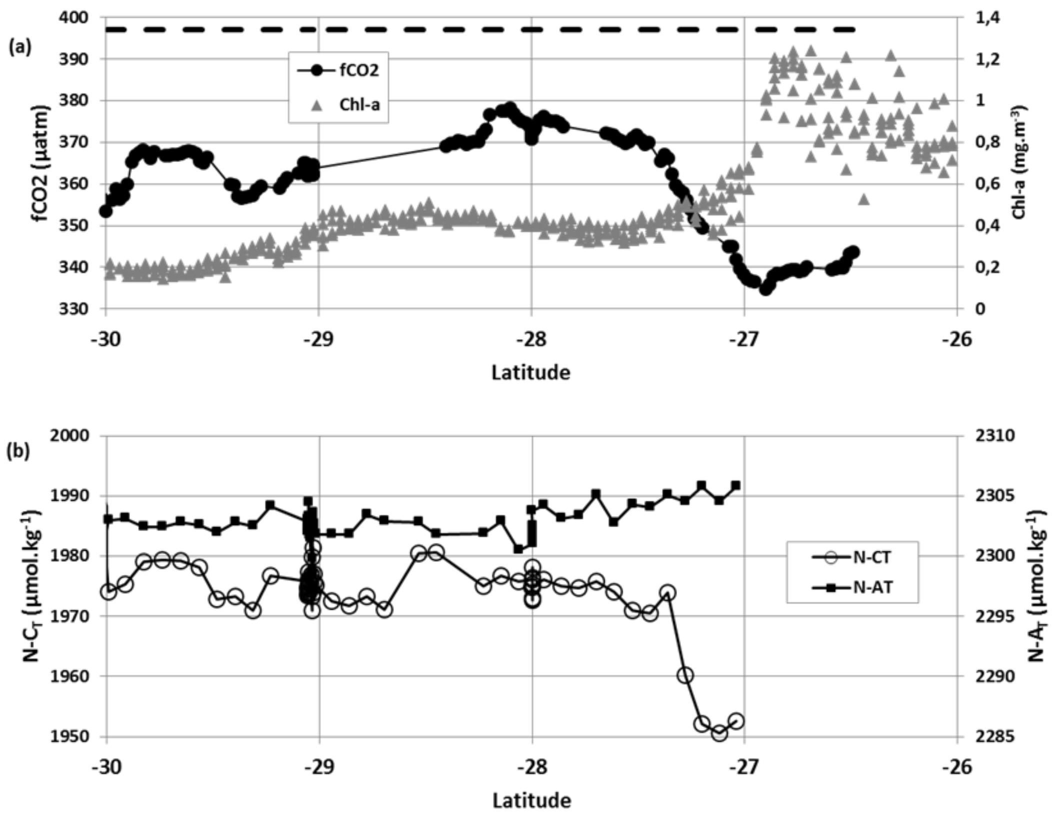

Figure 4: ΔfCO_2 (µatm) ($\Delta fCO_2 = fCO2_{ocean}-fCO2_{atm}$) and sea surface Chl-a ($mg.m^{-3}$) distribution in January 2020 (black) and February 2005 (orange) along the same track around 54°E in the South-Western Indian Ocean. Here Chl-a is in log10 scale and inverted. In 2020 when the SEMB was particularly strong ΔfCO_2 was negative (ocean CO_2 sink), whereas in 2005 when the bloom was small, ΔfCO_2 was close to 0 or positive (ocean CO_2 source).

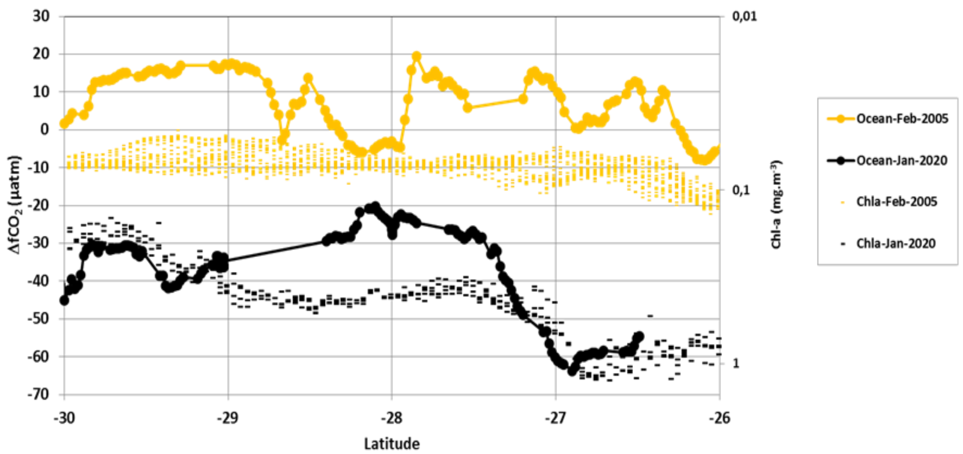

Figure 5: Time-series of anthropogenic CO_2 concentrations (C_{ant}) estimated in subsurface (layer 100-250m) in the region 26-30°S/55°E from the GLODAPv2-2021 data product (Lauvset et al, 2021,a,b) completed with OISO cruises in 2012-2018 (location of selected stations in the insert map). The figure shows the C_{ant} concentrations calculated for each sample (black dots) and the C_{ant} averaged in the layer 100-250m for each period (grey triangles). Over the period 1978-2020, the C_{ant} long-term trend is +1.05 (± 0.08) µmol.kg^{-1}.yr^{-1} (dashed grey line).

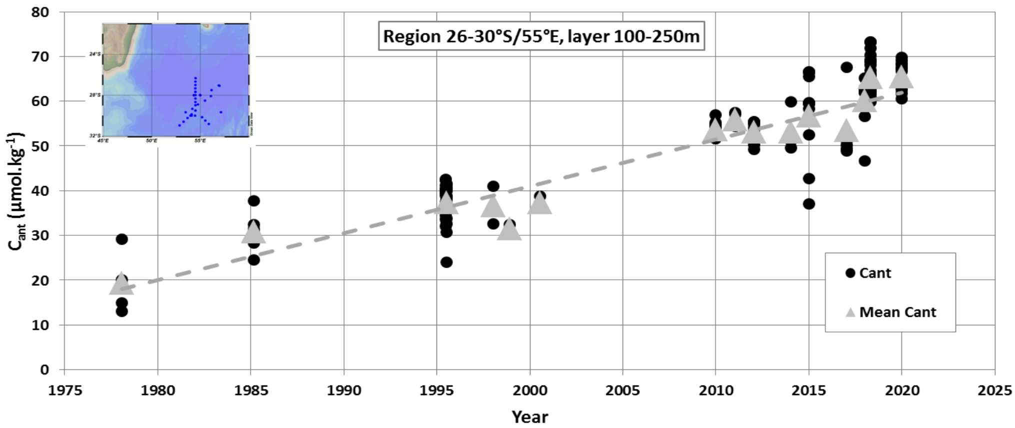

Figure 6: Relationship of A_T (µmol.kg^{-1}) versus Salinity deduced from surface A_T data (n= 3400) obtained during OISO cruises in 1998-2020 in the South-Western Indian Ocean. For the subtropics we have selected the data in the region 35°S-20°S/50°E-70°E (track of cruises shown in the insert map). The relationship (red dashed) is A_T = 62.1601 * SSS +123.1 and is used to calculate C_T concentrations in this region (Fig. 7). A_T data are available at NCEI/OCADS (https://www.ncei.noaa.gov/access/ocean-carbon-data-system/oceans/VOS_Program/OISO.html).

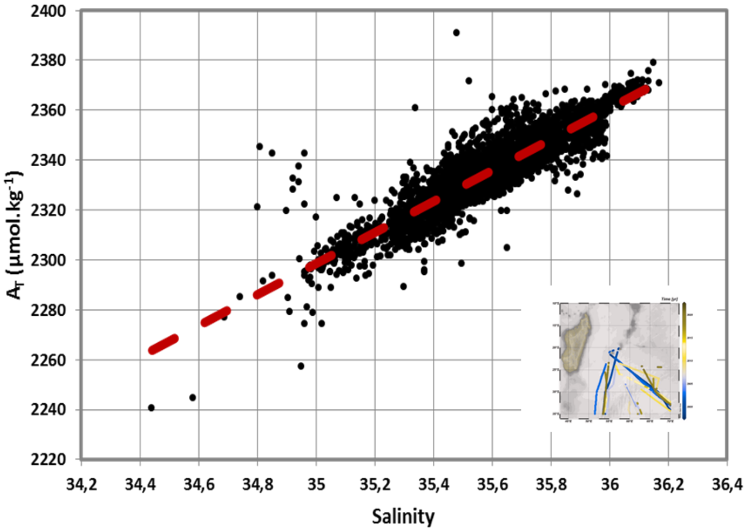

Figure 7: Time-series of salinity normalized C_T (N-C_T black dots) and their monthly mean (grey triangles) in the box 27°S-28°S/55°E (insert map) calculated with fCO_2 observations (see Fig. 2) and reconstructed A_T from salinity (Figure 6). The figure shows data for the months of January and February (data available from 1991 to 2020 for austral summer). Over the period 1991-2019, the N-C_T trend is +0.70 (± 0.24) $\mu mol.kg^{-1}.yr^{-1}$ (dashed grey line) reflecting in part the anthropogenic CO_2 uptake. Note the low N-C_T in January 2020 in the SEMB compared to previous years with some values around 1950 $\mu mol.kg^{-1}$ in 2020 as low as N-C_T calculated in 1991. The N-C_T concentration in the same region derived from the climatology of Takahashi et al (2014) is also plotted (orange diamond for the reference year 2005) as well as the climatological value for year 2020 after correcting for anthropogenic CO_2 (red diamond).

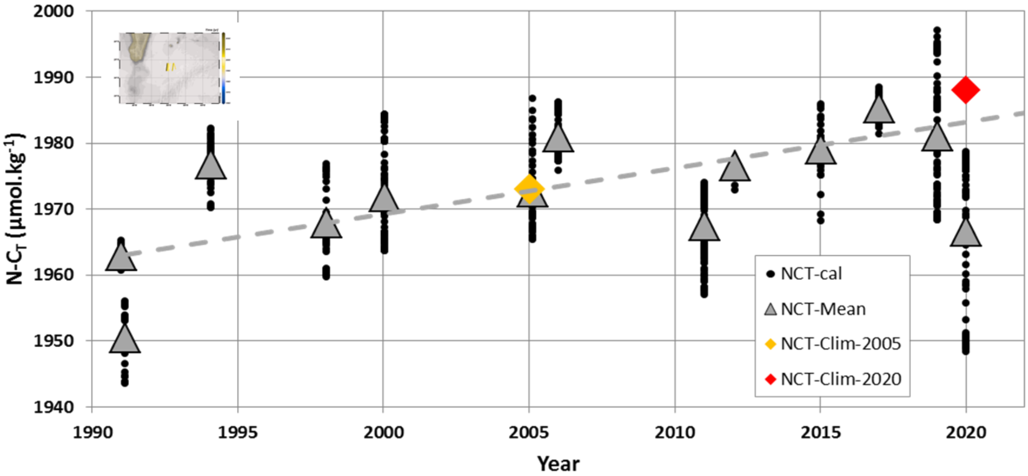

Figure 8: Sea surface silicate concentration (Si, µmol.kg^{-1}, black circles, scale on the left), N_2 fixation rate (N_2-fix, nmol N.L^{-1}.d^{-1}, open squares, scale on the right) measured in January 2020 (OISO-30 cruise) and Chl-a (mg.m^{-3}, grey triangles, scale on the left) from MODIS (4x4 km) along the cruise track. The low Si concentration (0.6 µmol.kg^{-1}) recorded around 27°S was linked to higher Chl-a (up to 1.2 mg.m^{-3}) in the SEMB.

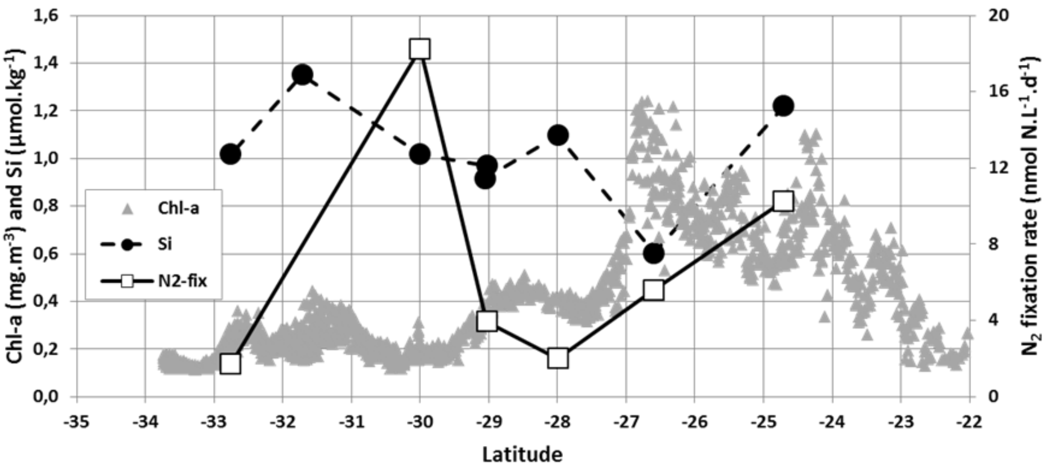

Figure 9: The relationship between N-C_T (μmol.kg^{-1}) and SST in surface waters based on OISO cruises observations in the south-western Indian Ocean in austral summer 2017, 2018, 2019 and 2020 along the same repeated track (insert map). In January 2020 during the strong SEMB the N-C_T/SST relationship (black dots and black line) was much sharper than in 2017-2019 (grey dots and grey line) indicative of N_2-fix production in nitrate depleted waters (e.g. Ko et al 2018).

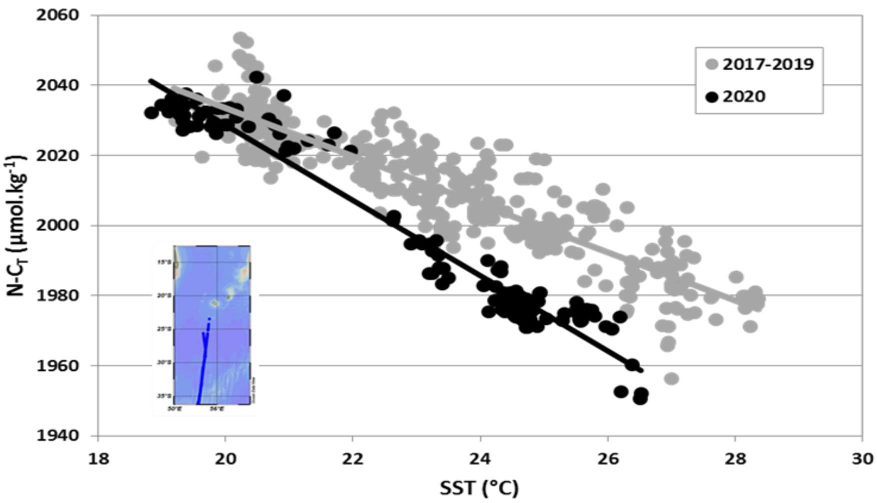

Figure 10: Maps of Chl-a (mg.m^{-3}), pCO2 (µatm) and the air-sea CO_2 fluxes (mmol.m^{-2}.d^{-1}) in the South-Western Indian Ocean in December 2018 (left) and December 2019 (right). In December 2019 when the SEMB was particularly strong, the pCO_2 was lower and air-sea CO_2 fluxes were negative (ocean sink, in blue), whereas in December 2018 when the bloom was small, the fluxes were near equilibrium or positive in this region (ocean source, yeallow-brown). Chl-a data downloaded at https://resources.marine.copernicus.eu/ (OCEANCOLOUR_GLO_CHL_L4_REP_OBSERVATIONS_009_093), last access, 10-April-2021. Figures produced with ODV (Schlitzer, 2013).

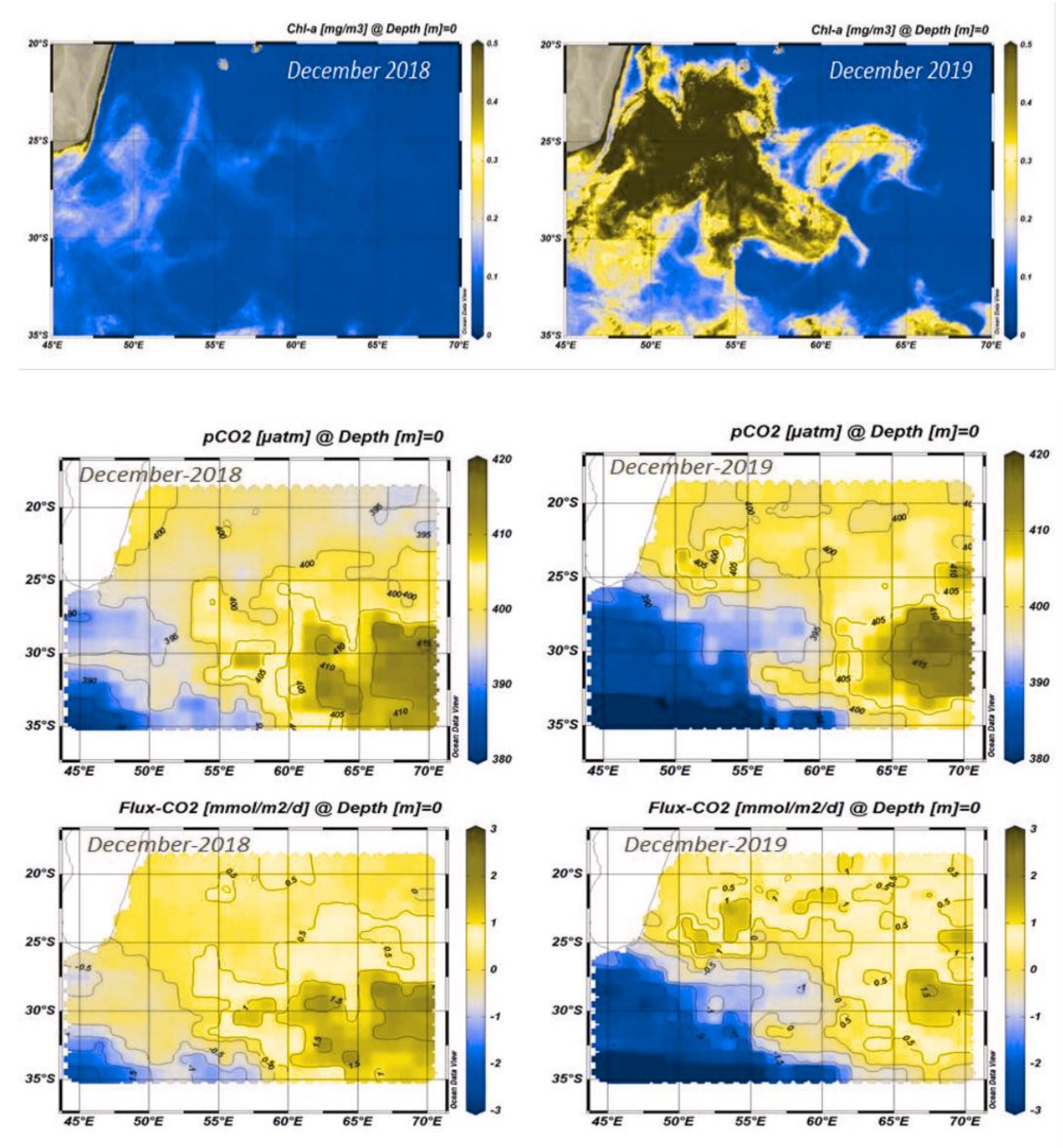

Figure 11: Annual air-sea CO_2 flux ($TgC.yr^{-1}$) in the South-Western Indian Ocean (region 25-30°S/50-60°E) for the period 1996-2019 from the CMEMS-LSCE-FFNN model. The carbon uptake progressively increased after 2007 with a maximum CO_2 sink estimated in 2019 when the SEMB was particularly strong.